

LEARNER: A Transfer Learning Method for Low-Rank Matrix Estimation

Sean McGrath¹, Cenhao Zhu², Min Guo³, and Rui Duan³

¹Department of Population Medicine, Harvard Medical School and Harvard Pilgrim Health Care Institute, Boston, MA, USA

²Operations Research Center, Massachusetts Institute of Technology, Cambridge, MA, USA

³Department of Biostatistics, Harvard T.H. Chan School of Public Health, Boston, MA, USA

Abstract

Low-rank matrix estimation is a fundamental problem in statistics and machine learning. In the context of heterogeneous data generated from diverse sources, a key challenge lies in leveraging data from a source population to enhance the estimation of a low-rank matrix in a target population of interest. One such example is estimating associations between genetic variants and diseases in non-European ancestry groups. We propose an approach that leverages similarity in the latent row and column spaces between the source and target populations to improve estimation in the target population, which we refer to as LatEnt spAce-based tRansfer lEaRning (LEARNER). LEARNER is based on performing a low-rank approximation of the target population data which penalizes differences between the latent row and column spaces between the source and target populations. We present a cross-validation approach that allows the method to adapt to the degree of heterogeneity across populations. We conducted extensive simulations which found that LEARNER often outperforms the benchmark approach that only uses the target population data, especially as the signal-to-noise ratio in the source population increases. We also performed an illustrative application and empirical comparison of LEARNER and benchmark approaches in a re-analysis of a genome-wide association study in the BioBank Japan cohort. LEARNER is implemented in the R package `learner`.

1 Introduction

For many real-world datasets, it has been shown that the underlying signal structures typically lie in a lower-dimensional subspace [1]. Consequently, low-rank matrix estimation plays a central role in numerous analyses with applications spanning genetics, psychology, atmospheric sciences, chemistry, economics, and others [2]. For example, it is widely used in matrix completion for missing data imputation [3, 4, 5, 6], semantic analyses such as word embeddings (e.g., Word2Vec) [7, 8], topic modeling in natural language processing [9], fine-tuning large language models [10], and uncovering the genetic basis of complex diseases by integrating genome-wide association studies (GWAS) summary statistics [11, 12]. A key feature in low-rank estimation problems is that the low-rank matrix can be expressed in terms of latent features in the row and column spaces (e.g., latent genetic and disease factors in Sakaue et al. [12] and Tanigawa et al. [11]), which can be of interest themselves as well as used in downstream analyses such as data visualization and clustering. Common statistical methods for low-rank estimation problems include truncated singular value decomposition (SVD) methods [13, 14] and a number of its variants and special cases, including principal component analysis (PCA) methods [15], nonnegative matrix factorization methods [16], and other factorization methods [2].

With the growing availability of high-dimensional, complex, and heterogeneous datasets, there is an increasing demand for methods that integrate and analyze multiple datasets simultaneously. In biomedical

research, for instance, data availability often varies significantly across populations, with certain groups being underrepresented compared to others that are more extensively studied. This underrepresentation limits the generalizability and applicability of research findings across diverse populations, reducing the effectiveness of medical interventions and models in underrepresented demographic settings [17, 18, 19]. To address this challenge, researchers are increasingly exploring ways to leverage data or models from well-studied populations to enhance understanding and improve analysis for populations with limited data. This approach, commonly referred to as transfer learning in the machine learning literature [20], has shown promise in bridging these gaps and enabling more equitable biomedical advancements [21, 22, 23, 24].

In this paper, we address the problem of low-rank matrix estimation on a target population. While low-rank estimation problems have been extensively studied, limited attention has been given to scenarios where data from a target population is underrepresented or of low quality. In such cases, leveraging data from a well-studied source population might improve the low-rank estimation for the target population, where the challenges lies in how to effectively utilize such auxiliary data while accounting for the inherent differences between the source and target populations.

Current research has explored matrix factorization methods in settings involving multiple data sources [25, 26, 27, 28, 29]. Oba et al. [25] proposed multi-source PCA methods when only the noise level within the populations differ. Fan et al. [26] proposed a multi-source PCA method when the populations share the same leading eigenspaces (see also Duan et al. [27]). Shi and Al Kontar [28] recently proposed a multi-source PCA method for populations that exactly share a given number of principal components. Li et al. [29] developed a multi-source PCA method based on similar assumptions as Shi and Al Kontar [28] regarding the similarity between the populations. A limitations of these methods is that they are based on relatively strong assumptions on the similarity between the populations.

We propose an approach called *LatEnt spAce-based tRaNsfer lEaRning* (LEARNER) for improving estimation of a low-rank matrix in underrepresented target populations that allows for flexible patterns of heterogeneity between the source and target populations. This approach leverages similarity in the latent factors in the underlying low-rank structure between the two populations through a penalized optimization problem, which penalizes differences in the latent row and column spaces between the two populations. We propose a scalable numerical optimization approach. Further, we propose a cross-validation approach to select the appropriate degree of transfer learning between the populations. We also present a tuning-parameter free approach under certain assumptions on the similarity between the latent spaces of the target and source populations.

The rest of the paper is organized as follows. In Section 2, we describe LEARNER and benchmark approaches without transfer learning. We evaluate the performance of LEARNER and benchmark approaches in simulation studies in Section 3. We apply LEARNER and compare it to benchmark approaches in a data application based on estimating genetic associations in a Japanese population in Section 4. We conclude with a discussion in Section 5.

2 Methods

2.1 Model and notation

Let $\Theta_k \in \mathbb{R}^{p \times q}$ denote the underlying low rank signal matrix in the population k , where $k = 0$ corresponds to the target population and $k = 1$ corresponds to the source population. Instead of observing Θ_k directly, we assume that we only observe a noisy-version estimate Y_k in population k . In our running example, Θ_k is the underlying association between a set of p genetic variants and q phenotypes, where Y_k may be obtained from reported summary statistics or may be calculated from individual-level data, which is subject to estimation error.

Consider the model

$$Y_0 = \Theta_0 + Z_0 \tag{1}$$

$$Y_1 = \Theta_1 + Z_1 \tag{2}$$

where Z_0 and Z_1 are mean-zero noise matrices with $\mathbb{E}\|Z_k\|_{op} = \sigma_k$ for $k = 0, 1$. We denote the signal strength in each population by $\theta_k = \lambda_{\min}(\Theta_k)$, where λ_{\min} denotes the smallest singular value of a matrix. We focus on a setting where estimating Θ_0 in the target population is more challenging, due to issues such as underrepresentation in the original cohort used to derive summary statistics or low data quality, which may result in weaker signal strength or higher levels of noise in Y_0 compared to Y_1 .

We assume that Θ_0 and Θ_1 have rank r where $r \leq \min\{p, q\}$. This implies that Θ_0 admits the decomposition $\Theta_0 = UV^\top$ for some $U \in \mathbb{R}^{p \times r}$ and $V \in \mathbb{R}^{q \times r}$. Under certain identifiability conditions, the columns of $U \in \mathbb{R}^{p \times r}$ and $V \in \mathbb{R}^{q \times r}$ can be interpreted as latent genotypic and phenotypic factors, respectively (e.g., see [12]). Specifically, $U_{i\ell}$ can be interpreted as a measure of the relative importance of the i th genetic variant to the ℓ th latent genotypic factor. Similarly, $V_{j\ell}$ can be interpreted as a measure of the relative importance of the j th phenotype to the ℓ th latent phenotypic factor. The association between the i th variant and the j th phenotype in the target population can then be expressed as $\Theta_{0,ij} = \sum_{\ell=1}^r U_{i\ell}V_{j\ell}$. While the target of inference is Θ_0 , measures of the relative importance of the genetic variants and phenotypes to the latent components based on U and V can sometimes be of interest themselves. In the data analysis in Section 4, we further discuss and illustrate measures of relative importance of the genetic variants and phenotypes to the latent components.

The following subsections describe methods to estimate Θ_0 .

2.2 Approach without transfer learning from the source population

The *truncated singular value decomposition (SVD)* is a conventional approach to estimate Θ_0 which leverages the low-rank structure of Θ_0 but does not leverage the source population data. The truncated SVD of Y_0 with rank r , denoted by $W_{0,r}$, is the best rank r approximation of Y_0 in the sense that

$$W_0 = \arg \min_{W: \text{rank}(W)=r} \|W - Y_0\|_F^2.$$

We can express W_0 by $W_0 = \hat{U}_0 \hat{\Lambda}_0 \hat{V}_0^\top$ where $\hat{U}_0 \in \mathbb{R}^{p \times r}$ and $\hat{V}_0 \in \mathbb{R}^{q \times r}$ are orthonormal matrices and $\hat{\Lambda}_0 \in \mathbb{R}^{r \times r}$ is a diagonal matrix. The columns of \hat{U}_0 and \hat{V}_0 are referred to as the left and right singular vectors of Y_0 , respectively, and the entries of $\hat{\Lambda}$ are referred to as the singular values of Y_0 .

A crucial question in the truncated SVD approach is how to select the rank r . We discuss approaches for rank selection in Section 2.3.4.

2.3 Latent space-based transfer learning

We propose an approach to estimate Θ_0 that leverages (i) the low-rank structure of Θ_0 and (ii) the similarity in the latent row and column subspaces between the source and target populations. This approach uses a rank r approximation of Y_0 which penalizes discrepancies in the span of the latent row and column spaces between the source and target populations. By penalizing discrepancies based the span of the latent row and column spaces rather than based on the singular vectors themselves, this approach can effectively borrow information from the source population under weaker conditions on the similarity between the populations (e.g., not requiring that the order of the singular vectors to be the same between the populations). A detailed description of our approach is below.

First, we estimate the genotypic and phenotypic latent subspaces in the source population, which involves the following notation. Let $U_k \Lambda_k V_k^\top$ denote the truncated SVD of Θ_k with rank r . Then $\mathcal{P}(U_k) := U_k U_k^\top$ is a projection matrix onto the space of latent genotypic factors in population k . Similarly, $\mathcal{P}(V_k) := V_k V_k^\top$ is a projection matrix onto the space of latent phenotypic factors in population k . We estimate $\mathcal{P}(U_1)$ and $\mathcal{P}(V_1)$ based on the rank r truncated SVD of Y_1 (i.e., by $\mathcal{P}(\hat{U}_1)$ and $\mathcal{P}(\hat{V}_1)$, where $\hat{U}_1 \hat{\Lambda}_1 \hat{V}_1^\top$ denotes the rank r truncated SVD of Y_1).

The LEARNER estimator of Θ_0 is given by $\hat{\Theta}_0^{\text{LEARNER}} = \tilde{U} \tilde{V}^\top$ where (\tilde{U}, \tilde{V}) is the solution to the following optimization problem

$$\arg \min_{U \in \mathbb{R}^{p \times r}, V \in \mathbb{R}^{q \times r}} \left\{ \|UV^\top - Y_0\|_F^2 + \lambda_1 \|\mathcal{P}_\perp(\hat{U}_1)U\|_F^2 + \lambda_1 \|\mathcal{P}_\perp(\hat{V}_1)V\|_F^2 + \lambda_2 \|U^\top U - V^\top V\|_F^2 \right\} \quad (3)$$

where $\mathcal{P}_\perp(\hat{U}_1) = I - \mathcal{P}(\hat{U}_1)$ and $\mathcal{P}_\perp(\hat{V}_1) = I - \mathcal{P}(\hat{V}_1)$. Note that $\mathcal{P}_\perp(\hat{U}_1)$ can be interpreted as the projection matrix onto the orthogonal complement of the space of the latent genotypic factors in the source population; $\mathcal{P}_\perp(\hat{V}_1)$ has an analogous interpretation for the phenotypic factors. Therefore, the second and third terms of (3) can be interpreted as penalizing difference in the latent genotypic and phenotypic spaces, respectively, between the target and source populations. The last term in (3) balances the sizes of U and V .

Another way of interpreting (3) is that it interpolates between the SVDs of Y_0 and Y_1 . In particular, the truncated SVD of Y_0 is a special case of LEARNER when $\lambda_1 = 0$ and the truncated SVD of Y_1 is a special case when $\lambda_1 = \infty$. In this regard, LEARNER adapts to the level of heterogeneity between the two populations when using suitable λ_1, λ_2 values. Note that we let the second and third terms have identical penalties (i.e., λ_1). In cases where one believes that the degree of similarity between the latent genotypic factors between the two populations is highly different than the degree of similarity between the latent phenotypic factors between the populations, one can use different penalties on the second and third terms.

In the following subsections, we outline how to numerically solve (3), how to adapt the approach in the presence of missing data, how to select λ_1 and λ_2 , and how to select the rank.

2.3.1 Numerical optimization approach

To numerically solve (3), we consider an alternating minimization strategy, which has been commonly employed to solve similar matrix estimation problems [30, 31, 32]. Given an initial point, this approach updates U by minimizing the objective function (via a gradient descent step) treating V as fixed. Then, in the same manner, V is updated treating U as fixed. These updates of U and V are repeated until convergence.

Algorithm 1 summarizes the numerical optimization approach used to solve (3). Throughout Algorithm 1, f denotes the objective function in (3). For the stopping criteria, we terminate the for loop whenever any of the following conditions occur: (i) the value of objective function does not significantly change between iterations (i.e., $|\epsilon_t - \epsilon_{t-1}|$ is sufficiently small), (ii) a maximum number of iterations is reached, or (iii) the value of the objective function begins to diverge (e.g., $\epsilon_t > 10\epsilon_0$). The implementation of Algorithm 1 involves computing gradients of f with respect to U and V . A straightforward calculation shows that these gradients are given by

$$\begin{aligned}\nabla_U f(U, V) &= 2(UV^\top V - Y_0 V) + 2\lambda_1 \mathcal{P}_\perp(\hat{U}_1)U + 4\lambda_2 U(U^\top U - V^\top V) \\ \nabla_V f(U, V) &= 2(VU^\top U - Y_0^\top U) + 2\lambda_1 \mathcal{P}_\perp(\hat{V}_1)V + 4\lambda_2 V(V^\top V - U^\top U).\end{aligned}$$

Algorithm 1 LEARNER

Input Target population data $Y_0 \in \mathbb{R}^{p \times q}$, source population data $Y_1 \in \mathbb{R}^{p \times q}$, rank $r \in \mathbb{R}$, regularization parameters $\lambda_1, \lambda_2 \in \mathbb{R}$, step size $c \in \mathbb{R}$

Output Estimate $\hat{\Theta}_0^{\text{LEARNER}} \in \mathbb{R}^{p \times q}$

function LEARNER($Y_0, Y_1, r, \lambda_1, \lambda_2, c$)

- 1: Initialize $U^{(0)} \in \mathbb{R}^{p \times r}, V^{(0)} \in \mathbb{R}^{q \times r}$ based on the SVD of Y_1
 - 2: Initialize $\epsilon_0 \leftarrow f(U^{(0)}, V^{(0)})$
 - 3: **for** $t = 1, 2, \dots$ **do**
 - 4: Update $U^{(t)} \leftarrow U^{(t-1)} - c \frac{\|U^{(t-1)}\|_F}{\|\nabla_U f(U^{(t-1)}, V^{(t-1)})\|_F} \nabla_U f(U^{(t-1)}, V^{(t-1)})$
 - 5: Update $V^{(t)} \leftarrow V^{(t-1)} - c \frac{\|V^{(t-1)}\|_F}{\|\nabla_V f(U^{(t)}, V^{(t-1)})\|_F} \nabla_V f(U^{(t)}, V^{(t-1)})$
 - 6: Update $\epsilon_t \leftarrow f(U^{(t)}, V^{(t)})$
 - 7: **end for**
 - 8: Set $t_{\text{best}} = \arg \min_t \epsilon_t$
 - 9: Set $\hat{\Theta}_0^{\text{LEARNER}} = U^{(t_{\text{best}})} V^{(t_{\text{best}})\top}$
-

2.3.2 Handling missing data

When Y_0 has missing data, we can adapt LEARNER as follows. Let Ω denote the set of the indices of the non-missing entries in Y_0 . We can solve the following optimization problem

$$\arg \min_{U, V} \left\{ \frac{1}{|\Omega|/pq} \sum_{(i,j) \in \Omega} ((UV^\top)_{ij} - Y_{0,ij})^2 + \lambda_1 \|\mathcal{P}_\perp(\hat{U}_1)U\|_F^2 + \lambda_1 \|\mathcal{P}_\perp(\hat{V}_1)V\|_F^2 + \lambda_2 \|U^\top U - V^\top V\|_F^2 \right\} \quad (4)$$

However, it will be convenient to re-express (4) as follows

$$\arg \min_{U, V} \left\{ \frac{1}{|\Omega|/pq} \|UV^\top - \tilde{Y}_0\|_F^2 + \lambda_1 \|\mathcal{P}_\perp(\hat{U}_1)U\|_F^2 + \lambda_1 \|\mathcal{P}_\perp(\hat{V}_1)V\|_F^2 + \lambda_2 \|U^\top U - V^\top V\|_F^2 \right\} \quad (5)$$

where \tilde{Y}_0 is given by

$$(\tilde{Y}_0)_{ij} = \begin{cases} (Y_0)_{ij} & \text{if } (i, j) \in \Omega \\ (UV^\top)_{ij} & \text{otherwise.} \end{cases}$$

We can then apply Algorithm 1 to solve (5), where the first term in $\nabla_U f(U, V)$ and $\nabla_V f(U, V)$ is now scaled by $\frac{1}{|\Omega|/pq}$.

Note that scaling the first term in these optimization problems by the percentage of non-missing entries of Y_0 becomes important when applying cross-validation to select λ_1 and λ_2 (see Section 2.3.3). This scaling allows the relative size of the first term to remain the same when varying the percentage of missing entries in Y_0 , such as when holding out one fourth of the entries in Y_0 in cross-validation versus when not holding out any entries in Y_0 in the application with the selected λ_1 and λ_2 .

2.3.3 Selecting the degree of transfer learning

We consider a cross-validation approach so that the method can adapt to the level of heterogeneity between the source and target populations and thus can protect against negative transfer. Specifically, we consider the following four-fold cross-validation approach to select λ_1 and λ_2 . To form the training and test data sets, we randomly partition the entries Y_0 into four equally sized subsamples. The training data sets are obtained by removing one of the four subsamples and the corresponding test data sets are based on the held out subsamples. In fold k , let Ω_k denote the indices of Y_0 used for the training set and Ω_k^\perp denote the indices of Y_0 used for the test set.

We consider a grid of values for λ_1 and λ_2 , denoted by \mathcal{S}_1 and \mathcal{S}_2 . For each $(\lambda_1, \lambda_2) \in \mathcal{S}_1 \times \mathcal{S}_2$, we apply LEARNER to the training data sets and evaluate their mean squared errors (MSEs) on the test data sets. That is, in validation set k , the MSE is given by

$$\text{MSE}(\lambda_1, \lambda_2, k) = \frac{1}{|\Omega_k^\perp|} \sum_{(i,j) \in \Omega_k^\perp} (\hat{\Theta}_{ij}^{\text{LEARNER}, \lambda_1, \lambda_2, k} - Y_{0,ij})^2. \quad (6)$$

where $\hat{\Theta}^{\text{LEARNER}, \lambda_1, \lambda_2, k}$ denote the LEARNER estimate from training set k . We select the value of $(\lambda_1, \lambda_2) \in \mathcal{S}_1 \times \mathcal{S}_2$ with the smallest MSE across all four validation data sets (i.e. $\frac{1}{4} \sum_{k=1}^4 \text{MSE}(\lambda_1, \lambda_2, k)$).

2.3.4 Selecting the rank

In applications of SVD methods such as in PCA, a conventional approach to select the number of latent components is the so-called scree plot method [33]. In this method, the data analyst plots the ordered singular values of the matrix and visually identifies where an elbow appears in the plot, selecting all components before the elbow. Other conventional methods are based on selecting the number of components such that the total

variance explained (i.e., the cumulative sum of the first \tilde{r} singular values) is sufficiently large, such as 95% of the total variance [15].

Rank selection in matrix estimation problems has been studied by a number of seminal works in the theoretical and methodological literature (see Donoho et al.[34] and references within). For the proposed LEARNER method, since we assume that the target and the source populations share the same rank r , we consider estimating r by applying the ScreeNOT [34] method to Y_1 . ScreeNOT selects an optimal value for hard thresholding the singular values of Y_1 . That is, for the hard thresholding estimator $W_{1,\theta} := \sum_{i:\hat{\lambda}_i > \theta} \hat{\lambda}_i \hat{u}_i \hat{v}_i^\top$, this approach selects the value of θ that minimize $\|W_{1,\theta} - \Theta_1\|_F^2$. Note that this approach allows for various noise structures, such as correlated noise across the rows and/or columns of Y_1 . In situations where the source population and the target population have distinct underlying ranks, r_0 and r_1 , respectively, rank estimation can be performed separately for each population. However, the difference in ranks introduces additional dissimilarity between the latent spaces, making the source data less useful, particularly when $r_1 < r_0$.

2.3.5 Summary

Algorithm 2 summarizes the complete LEARNER method, including the selection of the rank r and regularization parameters λ_1 and λ_2 .

Algorithm 2 LEARNER with Nuisance Parameter Selection

Input Target population data $Y_0 \in \mathbb{R}^{p \times q}$, source population data $Y_1 \in \mathbb{R}^{p \times q}$, set of candidate λ_1 values \mathcal{S}_1 , set of candidate λ_2 values \mathcal{S}_2 , step size $c \in \mathbb{R}$

Output Estimate $\hat{\Theta}_0^{\text{LEARNER}} \in \mathbb{R}^{p \times q}$

- 1: Apply ScreeNOT to Y_1 to select r
 - 2: **for** $k = 1, 2, 3, 4$ **do**
 - 3: Select training data set indices Ω_k
 - 4: Set $Y_0^{\text{train},k}$ by setting entries corresponding to Ω_k to missing values
 - 5: **end for**
 - 6: **for** $(\lambda_1, \lambda_2) \in \mathcal{S}_1 \times \mathcal{S}_2$ **do**
 - 7: **for** $k = 1, 2, 3, 4$ **do**
 - 8: Set $\hat{\Theta}_0^{\text{LEARNER},\lambda_1,\lambda_2,k} = \text{LEARNER}(Y_0^{\text{train},k}, Y_1, r, \lambda_1, \lambda_2, c)$
 - 9: Set $\text{MSE}(\lambda_1, \lambda_2, k)$ by applying (6)
 - 10: **end for**
 - 11: Set $\text{MSE}(\lambda_1, \lambda_2) = \frac{1}{4} \sum_{k=1}^4 \text{MSE}(\lambda_1, \lambda_2, k)$
 - 12: **end for**
 - 13: Set $(\lambda_1^{(\text{best})}, \lambda_2^{(\text{best})}) = \arg \min_{(\lambda_1, \lambda_2)} \text{MSE}(\lambda_1, \lambda_2)$
 - 14: Set $\hat{\Theta}_0^{\text{LEARNER}} = \text{LEARNER}(Y_0, Y_1, r, \lambda_1^{(\text{best})}, \lambda_2^{(\text{best})}, c)$
-

2.4 Direct projection LEARNER

When we have prior knowledge about the latent spaces of the genotypic and phenotypic factors are the same between the source and target populations (i.e., $\mathcal{P}(U_0) = \mathcal{P}(U_1)$ and $\mathcal{P}(V_0) = \mathcal{P}(V_1)$), we can consider a simpler estimation method than LEARNER. This approach estimates Θ_0 by directly projecting Y_0 onto the genotypic and phenotypic latent spaces learned from the source population, which we refer to as the *direct projection LEARNER (D-LEARNER)* approach. We can express this estimator as

$$\hat{\Theta}_0^{\text{D-LEARNER}} = \mathcal{P}(\hat{U}_1)Y_0\mathcal{P}(\hat{V}_1).$$

A key advantage of this approach is that it does not require selecting the tuning parameters λ_1 and λ_2 , which can be computationally expensive and statistically challenging in some settings (e.g., see Section 3.2). However, the projection method forces the target estimate to conform to the singular spaces of the

source, potentially increasing errors when the source population diverges significantly from the target. This alignment may not accurately reflect the characteristics of the target population, leading to distorted or misleading results.

3 Simulation study

3.1 Independent noise

Our first set of simulations consider the setting of independent noise. These simulations evaluate how the performance of the LEARNER and benchmark approaches is affected by the (i) similarity between the latent spaces of the source and target populations, (ii) signal-to-noise ratio in the source population, and (iii) rank r in the setting of independent noise. To characterize similarity between the latent spaces of the source and target populations in these simulations, we define the measures

$$\begin{aligned} d_U &:= \|\mathcal{P}(U_1) - \mathcal{P}(U_0)\|_F \\ d_V &:= \|\mathcal{P}(V_1) - \mathcal{P}(V_0)\|_F. \end{aligned}$$

3.1.1 Simulation design

We set $\Theta_0, \Theta_1 \in \mathbb{R}^{p \times q}$ with $(p, q) = (5000, 50)$ as follows. We considered $r \in \{4, 8\}$. We set Θ_0 by generating a $p \times q$ matrix with i.i.d. Normal(0, 1) entries and then performing a truncated SVD with rank r . We considered three scenarios for Θ_1 based on the similarity of the latent spaces of the source and target populations:

1. *High similarity*: We let Θ_1 have the same left and right singular vectors as Θ_0 but in different order. Specifically, we set Θ_1 by reversing the order of the singular values of Θ_0 . Note that $d_U = d_V = 0$ in this case.
2. *Moderate similarity*: We set Θ_1 by reversing the order of the singular values of Θ_0 and adding perturbations to the left and right singular vectors of Θ_0 . Specifically, we set the left singular vector matrix of Θ_1 by adding a matrix with i.i.d. Uniform($-\frac{1}{8\sqrt{p}}, \frac{1}{8\sqrt{p}}$) entries to the the left singular vector matrix of Θ_0 and orthonormalizing the resulting matrix. Similarly, we added i.i.d. Uniform($-\frac{1}{8\sqrt{q}}, \frac{1}{8\sqrt{q}}$) perturbations to the right singular vector matrix of Θ_0 and then orthonormalized the resulting matrix. This resulted in $d_U \approx 0.40, d_V \approx 0.42$ when $r = 4$ and $d_U \approx 0.57, d_V \approx 0.54$ when $r = 8$.
3. *Low similarity*: We set Θ_1 in the same manner as in the moderate similarity setting, except that the perturbations to the left singular vectors of Θ_0 were generated by Uniform($-\frac{1}{2\sqrt{p}}, \frac{1}{2\sqrt{p}}$) and the perturbations to the right singular vectors were generated by Uniform($-\frac{1}{2\sqrt{q}}, \frac{1}{2\sqrt{q}}$). This resulted in $d_U \approx 0.78, d_V \approx 0.83$ when $r = 4$ and $d_U \approx 1.11, d_V \approx 1.05$ when $r = 8$.

We simulated Y_0 and Y_1 by (1) and (2) with i.i.d. normal noise. To evaluate the effect of increasing the signal-to-noise ratio in the source population, we set $\sigma_0^2 = 0.1$ and considered $\sigma_1^2 \in \{\frac{\sigma_0^2}{10}, \frac{\sigma_0^2}{5}, \frac{\sigma_0^2}{3}, \sigma_0^2\}$.

In summary, there were $3 \times 4 \times 2 = 24$ different data generating scenarios by varying the similarity in the latent spaces of the source and target populations (3 levels), the variance of the noise in the source population (4 levels, $\sigma_1^2 \in \{\frac{\sigma_0^2}{10}, \frac{\sigma_0^2}{5}, \frac{\sigma_0^2}{3}, \sigma_0^2\}$), and the rank (2 levels, $r \in \{4, 8\}$). In each scenario, we performed 50 repetitions.

We compared the performance of the truncated SVD, LEARNER, and D-LEARNER methods. D-LEARNER and LEARNER estimated the rank using ScreeNOT. To serve as a benchmark, the true rank was used in the truncated SVD method. Details on the hyperparameters values used for LEARNER (e.g., candidate λ_1 and λ_2 values) these simulations are in Appendix A. For each method, we evaluated the average Frobenius norm of the estimation error (i.e., $\|\hat{\Theta}_0 - \Theta_0\|_F$) across the 50 repetitions.

3.1.2 Results

The simulation results are illustrated in Figure 1. In the high similarity simulation scenarios, the LEARNER and D-LEARNER methods performed best and similarly to each other. The performance of these two methods improved as the noise variance in the source population decreased.

Similar trends held in the moderate similarity scenario. LEARNER and D-LEARNER effectively leveraged the source population data to improve estimation of Θ_0 ; however, as one may expect, the degree of improvement for these methods – especially for D-LEARNER – was less compared to the scenarios with high similarity in the latent spaces.

The low similarity scenarios represent cases where only very limited information can be leveraged from the source population. As such, LEARNER only had a small improvement over the target-only truncated SVD approach. Since D-LEARNER assumes that the latent spaces between the source and target populations are identical, this approach performed worse than the target-only truncated SVD approach in these scenarios.

Trends were very similar between the rank 4 scenarios and the corresponding rank 8 scenarios. The estimation error of all three approaches that assume a low rank structure increased as the rank increased. The rank selection method used by LEARNER and D-LEARNER correctly selected the rank in each iteration in these simulations.

Note that, unlike the simulation settings with correlated noise (see Section 3.2), we do not include error bars in the figures illustrating the standard deviation of the estimation error because they are too small to be visible.

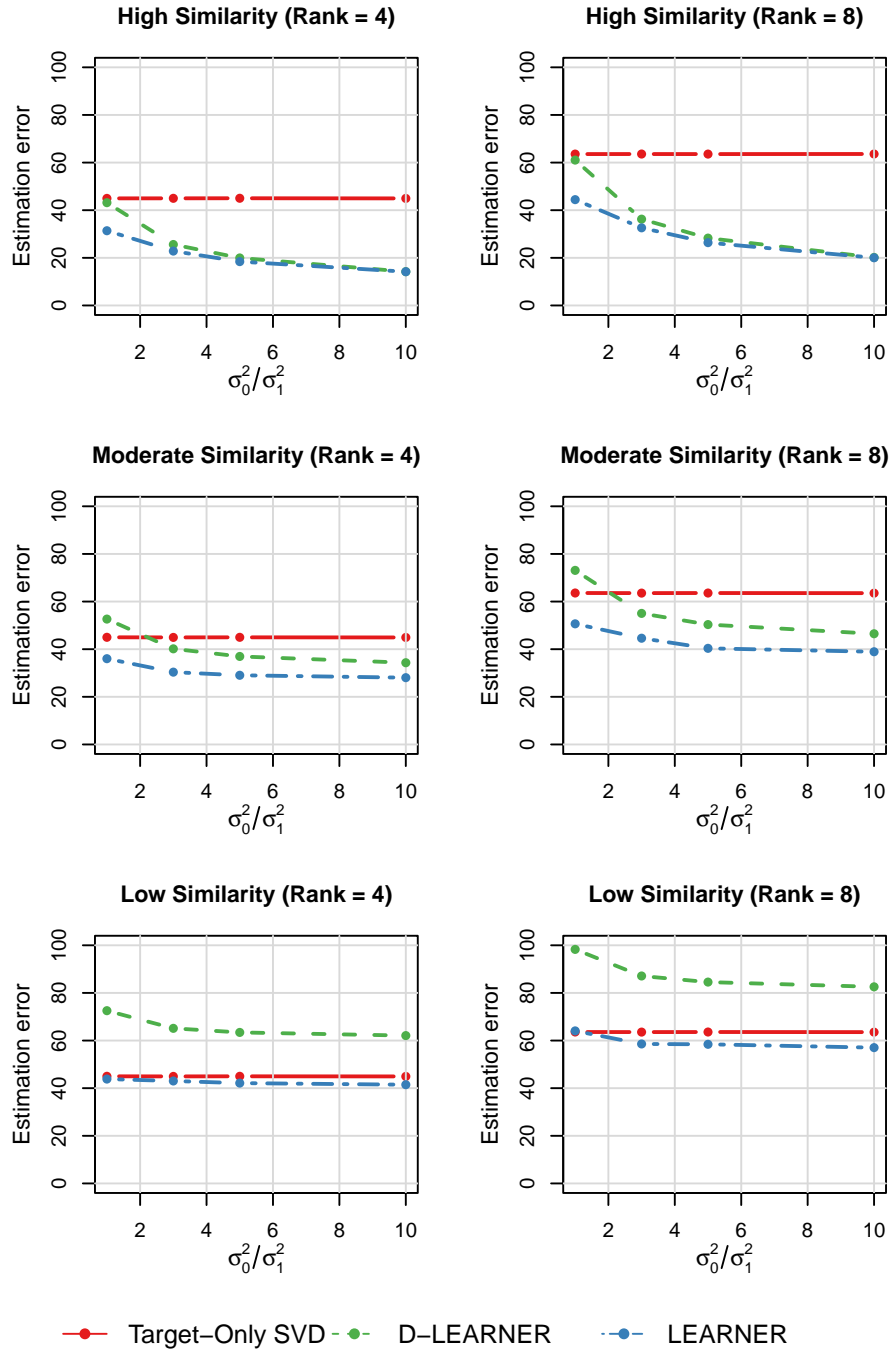


Figure 1: Simulation results in the independent noise scenarios.

3.2 Correlated noise

Our next set of simulations explore how the performance of the LEARNER and benchmark approaches are affected by correlated noise.

3.2.1 Simulation design

We set Θ_0 the same as in the simulations with independent noise (i.e., Section 3.1.1), and we set Θ_1 as in the high similarity, moderate similarity, and low similarity scenarios described in the independent noise simulations. We fixed the rank $r = 4$.

We simulated Y_0 and Y_1 by equations (1) and (2), although we now consider correlated noise settings. Letting $Z_{0,j}^\top$ and $Z_{1,j}^\top$ denote the j th columns of Z_0 and Z_1 respectively, we considered that $Z_{0,j}^\top \stackrel{\text{i.i.d.}}{\sim} \text{Normal}(0, \Sigma_0)$ and $Z_{1,j}^\top \stackrel{\text{i.i.d.}}{\sim} \text{Normal}(0, \Sigma_1)$. We let Σ_0 and Σ_1 have exchangeable covariance structures with a correlation of ρ ($\rho \in \{0.1, 0.25, 0.5\}$). That is, we let $\Sigma_{0,j_1,j_2} = \rho^{I(j_1 \neq j_2)} \sigma_0^2$ and $\Sigma_{1,j_1,j_2} = \rho^{I(j_1 \neq j_2)} \sigma_1^2$. As in the simulations with independent noise, we fixed $\sigma_0^2 = 0.1$ and considered $\sigma_1^2 \in \{\frac{\sigma_0^2}{10}, \frac{\sigma_0^2}{5}, \frac{\sigma_0^2}{3}, \sigma_0^2\}$.

In summary, there were $3 \times 3 \times 4 = 36$ different data generating scenarios by varying the similarity in the latent spaces of the source and target populations (3 levels), correlation ($\rho \in \{0.1, 0.25, 0.5\}$) and variance of the noise in the source population ($\sigma_1^2 \in \{\frac{\sigma_0^2}{10}, \frac{\sigma_0^2}{5}, \frac{\sigma_0^2}{3}, \sigma_0^2\}$).

We applied the same methods as described in the simulations with independent noise, and evaluated the average Frobenius norm of the estimation error across the 50 repetitions. Appendix A contains details on the hyperparameter values used by LEARNER in these simulations.

3.2.2 Results

The simulation results in the settings with high similarity in the latent spaces are summarized in the top row of Figure 2. D-LEARNER performed best in these scenarios, especially when the correlation was large. Its estimation error was not strongly affected by the degree of correlation. While LEARNER also improved on the target-only SVD approach, it did not perform as well as D-LEARNER. This may be attributed to selecting too small λ_1 values due to the fact that the held-out data in cross-validation was correlated with the non-held-out data. The rank selection method used by LEARNER and D-LEARNER incorrectly selected a rank of 5 (recall that the true rank was 4) in each iteration in each of the scenarios.

Similar trends held in the simulation scenarios with moderate and low similarity. LEARNER and D-LEARNER often outperformed the target-only SVD approach. However, the correlation in the noise had a bigger impact on LEARNER than D-LEARNER, which is likely due to the cross-validation approach in LEARNER performing sub-optimally.

In Appendix A, we describe a variation of LEARNER that selects the tuning parameters (λ_1, λ_2) based on using an independent data set from the target population rather than by using held-out entries of Y_0 . We find that that this variation of LEARNER performs considerably better in correlated noise settings, generally outperforming the target-only SVD and D-LEARNER methods.

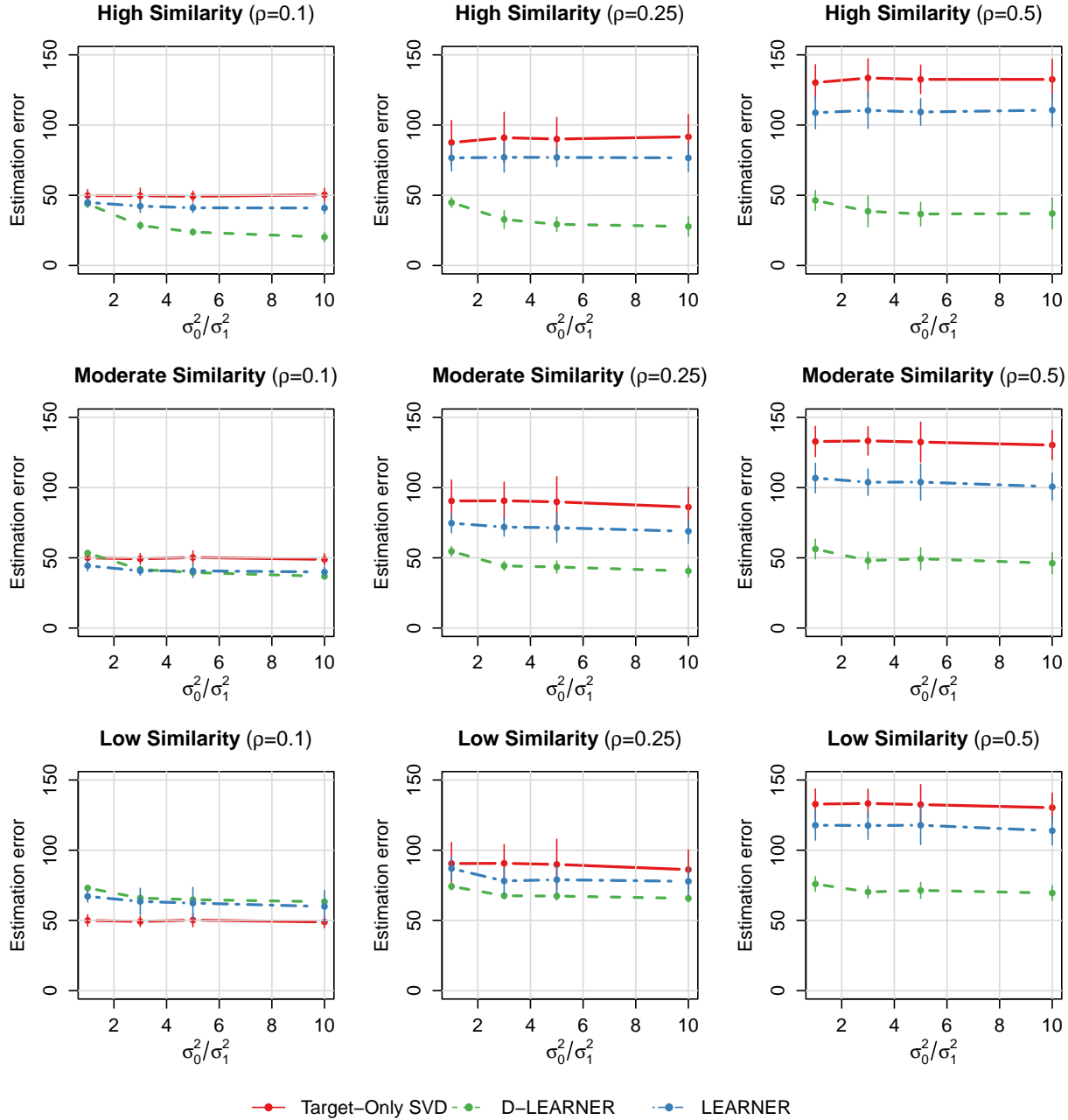


Figure 2: Simulation results under the correlated noise scenarios. The error bars correspond to the standard deviation of the estimation error across the 50 repetitions.

4 Data application

To illustrate an application of LEARNER and D-LEARNER, we obtained publicly available GWAS summary statistics from BioBank Japan (BBJ), UK Biobank (UKB), and FinnGen [12]. BBJ is a biobank containing clinical and genomic data of participants who were recruited from 12 medical institutes in Japan based

on having a diagnosis of one of 47 diseases [35]. UKB is a biobank with over 500,000 individuals from 22 assessment centers in the United Kingdom [36]. FinnGen combines data from Finland’s national health register (comprising all Finish residents since 1969) with a number of Finnish biobanks [37]. In our analyses, we consider the BBJ population to be the target population and combine the UKB European population and FinnGen European population to be the source population.

We selected disease endpoints (which we refer to as phenotypes throughout) and genetic variants in a manner generally consistent with that of Sakaue et al. [12]. We identified 145 phenotypes available in both the source and target populations. We then performed a standard screening procedure to select genetic variants significant in at least one of the datasets and at least one of the phenotypes. Additionally, genetic variants that are in high linkage disequilibrium (LD) were removed. We identified 27,124 genetic variants and 145 disease endpoints. The matrix Y_1 was formed based on performing an inverse variance weighted meta-analysis of the genetic associations across the UKB and FinnGen populations. For 27 of the phenotypes, source population data were only available from the UKB data and not the FinnGen data, in which case no meta-analysis was performed for these phenotypes. In total, the sample size for estimating the genetic associations was around 179,000 in the target population and 628,000 in the source population. A total of 0.006% of the entries in Y_0 were missing, and 0.102% of the entries in Y_1 were missing. See Appendix B.1 for additional details on the data processing. The code for processing the data and the processed data sets are available in the supplementary materials.

The original analysis in Sakaue et al. [12] concatenated the observed matrices in the source and target populations and applied the truncated SVD to the resulting matrix to estimate the latent representation of genetic variants and phenotypes. By combining the populations in this manner, this analysis treats different phenotypes within a population equivalently to phenotypes across different populations. Here, we adopt a transfer learning approach by applying the LEARNER and D-LEARNER methods to estimate Θ_0 .

4.1 Exploratory data analyses

In exploratory data analyses, we compared the latent components between the source and target populations based on Y_0 and Y_1 . These analyses focus on the projection matrices onto the latent phenotypic and genotypic spaces (i.e., $\mathcal{P}(\hat{U}_k)$ and $\mathcal{P}(\hat{V}_k)$ where \hat{U}_k and \hat{V}_k are the orthonormal left and right singular vector matrices, respectively, of Y_k) as well as the so-called phenotype and variant contribution scores [12]. The phenotype contribution score quantifies the relative importance of a given phenotype for a given latent component. Specifically, the phenotype contribution score of the i th phenotype for the ℓ th latent component of Y_k is given by $\hat{V}_{k,i,\ell}^2$, which ranges from 0 to 1. Similarly, the variant contribution score quantifies the relative importance of a given variant for a given latent component, which is defined as $\hat{U}_{k,i,\ell}^2$ for the i th variant and ℓ th latent component of Y_k .

To select the number of latent components in our analyses, we applied ScreeNOT to Y_1 (Figure 9 in Appendix B.2) which selected a rank of 8. We then computed the truncated SVD of Y_0 and Y_1 with the selected rank to compute the projection matrices and the phenotype and variant contribution scores.

Figure 3 compares the genotypic latent spaces between the target and source populations. We observe a high degree of similarity between the two populations. Figure 10 (Appendix B.2) illustrates the variant contribution scores in the target and source populations. The variants that had the highest contribution score in most of the latent components were on chromosome 6 in both populations (variant indices ranging from 8,947 to 12,222).

The projection matrices for the latent phenotypic components are given in Figure 4. There is a moderate degree of similarity between the target and source population. Figure 11 (Appendix B.2) illustrates the phenotype contribution scores in the two populations. In Tables 4 and 5 (Appendix B.2), we describe the top phenotypes (defined as phenotypes with the highest contribution scores) in the latent components in the target and source populations. Several phenotypes appear in the list of top phenotypes in both the target and source populations, such as type 2 diabetes, asthma, and Graves’ disease. We find that most latent components in the source population are characterized by well-known disease categories. For example, the third latent component is characterized by eye disorders (uveitis and iritis), the fourth latent component is

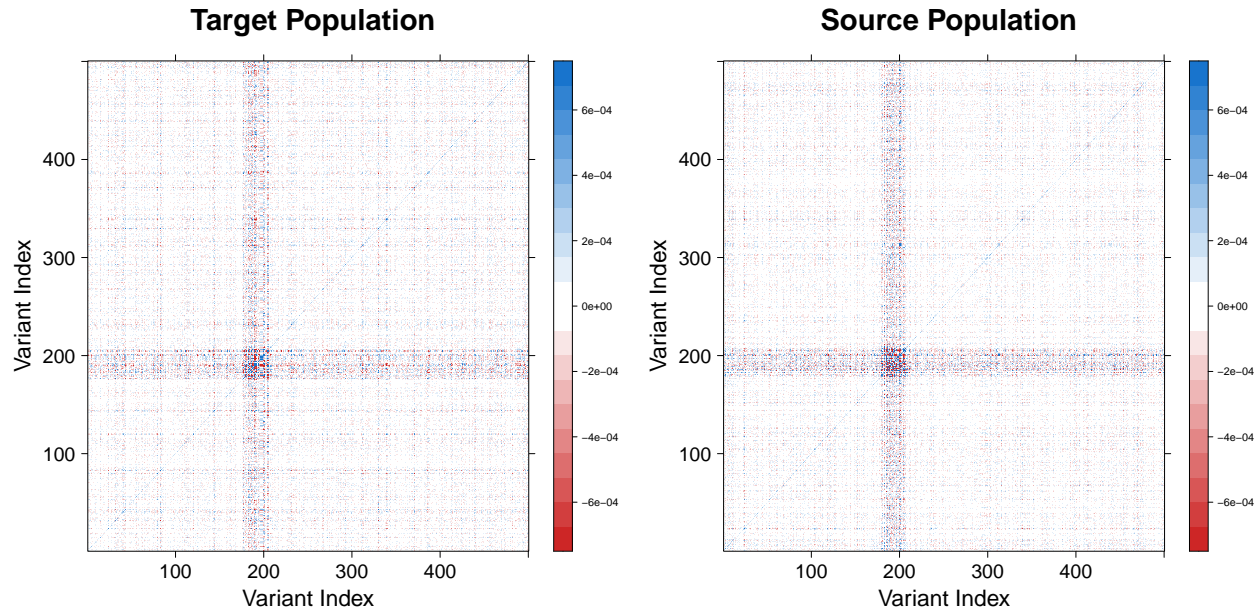


Figure 3: Heatmap of 500 randomly selected subset of rows and columns of $\mathcal{P}(\hat{U}_0)$ (left panel) and $\mathcal{P}(\hat{U}_1)$ (right panel). The 500 selected variants are ordered based on their chromosome and position number.

characterized by asthma (pediatric asthma, asthma), and the eighth latent component is characterized by angina pectoris (angina pectoris, stable angina pectoris, unstable angina pectoris). However, some of the latent components in the target population do not appear to correspond to a well-defined disease category. For example, component 8 has top phenotypes of asthma, chronic hepatitis B, iron deficiency anemia, uterine fibroid, and urticaria. We elaborate on the interpretation of the latent components when analyzing the LEARNER and D-LEARNER estimates in the following subsection.

4.2 LEARNER and D-LEARNER illustration

We applied LEARNER and D-LEARNER to estimate Θ_0 as described in Section 2.3. Appendix B.3 details the the hyperparameter used in LEARNER, and Appendix B.4 describes the results of the analyses selecting the tuning parameters for LEARNER and illustrates the convergence of the numerical optimization algorithm. The LEARNER and D-LEARNER estimates of Θ_0 are illustrated in Figure 5. We observe that the LEARNER and D-LEARNER estimates roughly have similar structures, although the LEARNER estimates often have larger magnitude than the corresponding D-LEARNER ones.

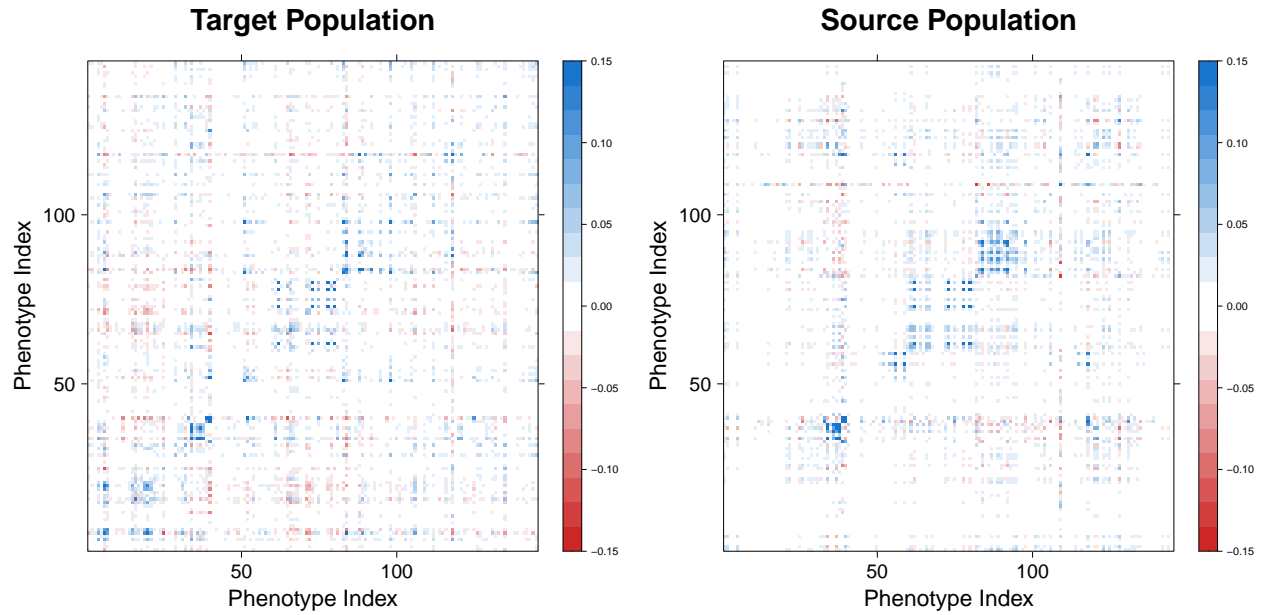


Figure 4: Heatmap of $\mathcal{P}(\hat{V}_0)$ (left panel) and $\mathcal{P}(\hat{V}_1)$ (right panel). The phenotypes are ordered based on their ICD-10 category.

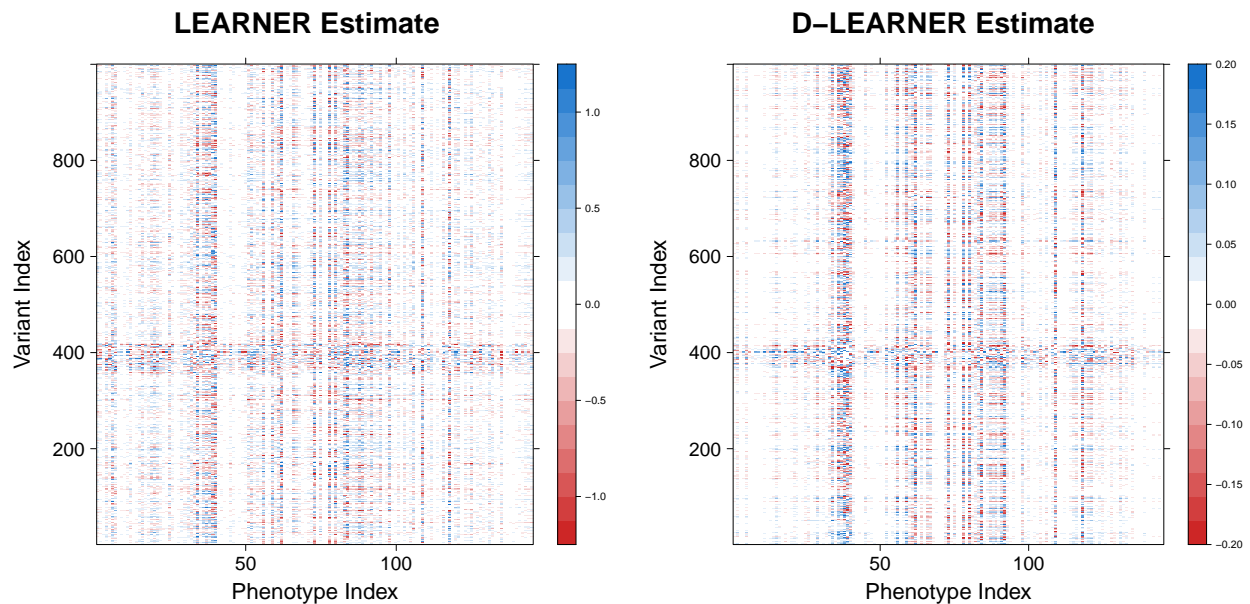


Figure 5: Heatmap of the LEARNER and D-LEARNER estimates of Θ_0 . A random subset of 1000 genetic variants (out of the 27,124) and all phenotypes are illustrated. The phenotypes are ordered based on their ICD-10 category, and the variants are ordered based on their chromosome and position number.

Figure 6 illustrates the phenotype and variant contribution scores in the target population based on the LEARNER estimate. To compute the contribution scores, we applied the singular value decomposition to the LEARNER estimate of Θ_0 . Similar to target-only truncated SVD approach, variants on chromosome 6

generally had the highest contribution scores for LEARNER. The top phenotypes in each latent component are listed in Table 1. For each latent factor, many of the top phenotypes were in the same disease class. For example, the second latent component is largely characterized by phenotypes relating to cardiovascular disorders, including (stable) angina pectoris, myocardial infarction, and type 2 diabetes. While there were a number of similarities in the phenotype contribution scores obtained from LEARNER compared to the target population truncated SVD approach (e.g., components 1 and 2 being characterized by autoimmune and cardiovascular disorders, respectively), there were also some key differences. LEARNER has a latent component characterized by eye disorders (uveitis and iritis) and has a component characterized by psoriasis vulgaris, which was found in the source population SVD approach but not the target population SVD approach.

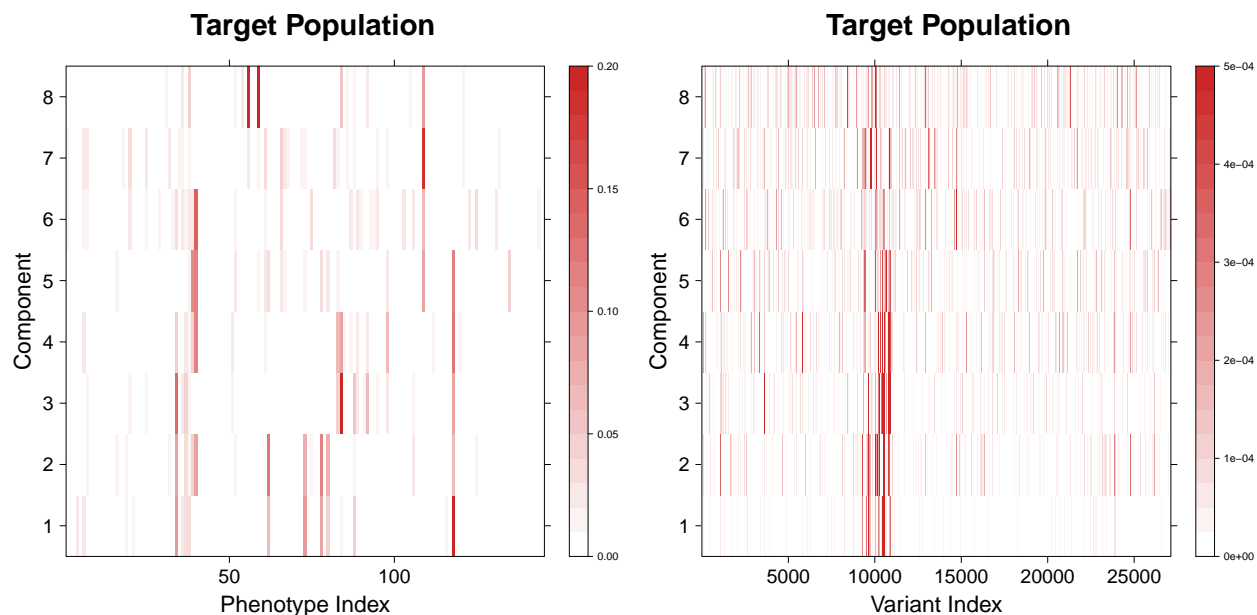


Figure 6: Heatmap of the matrix of phenotype (left panel) and variant (right panel) contribution scores in the target population based on LEARNER. The phenotypes are ordered based on their ICD-10 category, and the variants are ordered based on their chromosome and position number.

Figure 7 illustrates the phenotype and variant contribution scores in the target population for D-LEARNER. These contribution scores were calculated based on the singular value decomposition of the D-LEARNER estimate of Θ_0 . The top phenotypes for D-LEARNER are given in Table 2. Many latent factors were similar between the LEARNER and D-LEARNER estimates, such as latent factors for cardiovascular disorders, respiratory disorders, eye disorders, and psoriasis vulgaris. The D-LEARNER estimates of the phenotype contribution scores shared more similarities with the source population truncated SVD approach compared to LEARNER. For example, the first latent component of D-LEARNER had hypothyroidism and type 1 diabetes in the top two phenotypes, like the source population truncated SVD. This may be reasonably expected because D-LEARNER makes stronger assumptions on the similarity in the latent spaces between the source and target populations.

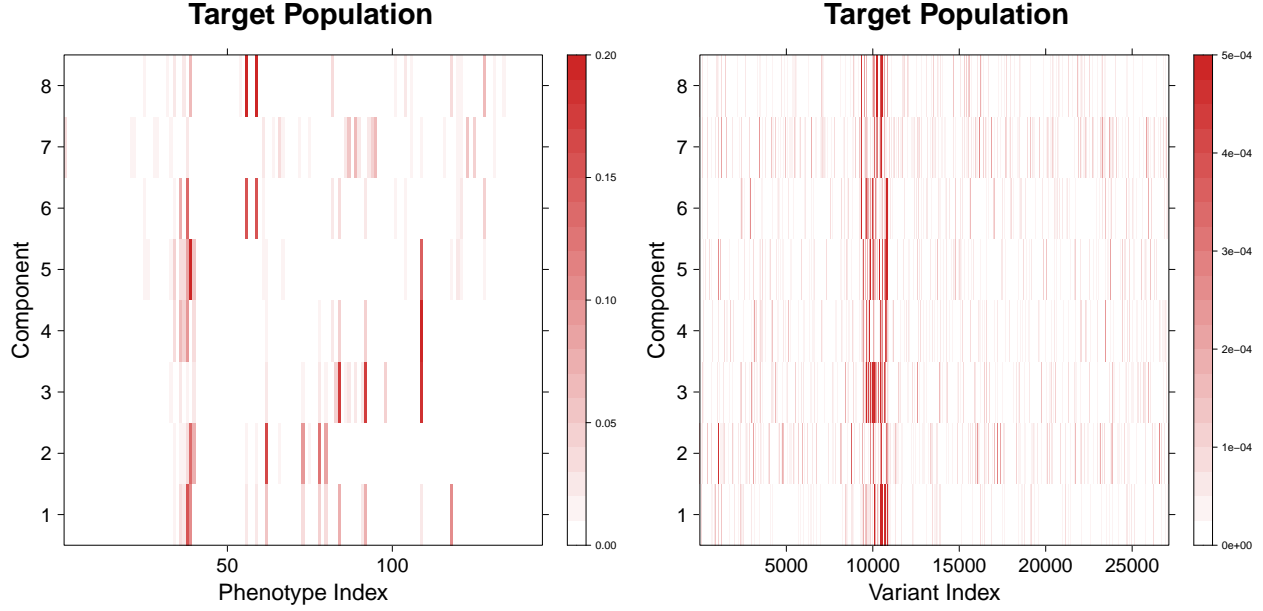


Figure 7: Heatmap of the matrix of phenotype (left panel) and variant (right panel) contribution scores in the target population based on D-LEARNER. The phenotypes are ordered based on their ICD-10 category, and the variants are ordered based on their chromosome and position number.

Table 1: Top phenotypes in each latent factor in the target population based on LEARNER. For each latent factor, we list the five phenotypes with the highest contribution scores. The phenotype contribution scores are in parentheses. The phenotypes related to the latent factor characterization are in bold text.

Factor	Characterization	Top phenotypes
1	Autoimmune disorders	Rheumatoid arthritis (0.21) , myocardial infarction (0.10), Graves' disease (0.09) , stable angina pectoris (0.08), angina pectoris (0.07)
2	Cardiovascular disorders	Angina pectoris (0.13) , stable angina pectoris (0.11) , type 2 diabetes (0.08) , Graves' disease (0.08), myocardial infarction (0.08)
3	Respiratory disorders	Asthma (0.24) , Graves' disease (0.13), rheumatoid arthritis (0.08), pediatric asthma (0.07) , chronic sinusitis (0.05)
4	Autoimmune/allergic conditions	Rheumatoid arthritis (0.13) , type 2 diabetes (0.12), asthma (0.09) , pollinosis (0.07) , allergic rhinitis (0.07)
5	Diabetes	Rheumatoid arthritis (0.12), type 2 diabetes (0.11) , type 1 diabetes (0.10) , psoriasis vulgaris (0.08), urolithiasis (0.04)
6	Diabetes	Type 2 diabetes (0.15) , psoriasis vulgaris (0.07), chronic renal failure (0.04), Graves' disease (0.03), chronic heart failure (0.03)
7	Psoriasis vulgaris	Psoriasis vulgaris (0.19) , chronic heart failure (0.04), varicose (0.04), atrial flutter/fibrillation (0.03), hepatic cancer (0.03)
8	Eye disorders	Uveitis (0.25) , iritis (0.24) , psoriasis vulgaris (0.10), asthma (0.05), hypothyroidism (0.05)

Table 2: Top phenotypes in each latent factor in the target population based on D-LEARNER. For each latent factor, we list the five phenotypes with the highest contribution scores. The phenotype contribution scores are in parentheses. The phenotypes related to the latent factor characterization are in bold text.

Factor	Characterization	Top phenotypes
1	Endocrine disorders	Hypothyroidism (0.16) , type 1 diabetes (0.11) , rheumatoid arthritis (0.10), asthma (0.07), pediatric asthma (0.07)
2	Cardiovascular disorders	Angina pectoris (0.17) , type 1 diabetes (0.14) , stable angina pectoris (0.13) , myocardial infarction (0.10) , unstable angina pectoris (0.09)
3	Respiratory/allergic conditions	Psoriasis vulgaris (0.19), pediatric asthma (0.17) , asthma (0.17) , allergic rhinitis (0.04) , pollinosis (0.04)
4	Psoriasis vulgaris	Psoriasis vulgaris (0.40) , hypothyroidism (0.09), Hashimoto’s disease (0.06), asthma (0.05), pediatric asthma (0.05)
5	Endocrine/metabolic disorders	Type 1 diabetes (0.25) , psoriasis vulgaris (0.14), hypothyroidism (0.08) , type 2 diabetes (0.06) , Graves’ disease (0.04)
6	Eye disorders	Iritis (0.15) , uveitis (0.15) , hypothyroidism (0.13), Hashimoto’s disease (0.07), IgA nephritis (0.04)
7	Respiratory disorders	Chronic obstructive pulmonary disease (0.07) , pneumonia (0.06) , chronic bronchitis (0.06) , acute renal failure (0.06), chronic renal failure (0.04)
8	Eye disorders	Iritis (0.22) , uveitis (0.22) , type 1 diabetes (0.07), IgA nephritis (0.06), varicose (0.04)

4.3 Empirical evaluation

We performed cross-validation analyses to compare the performance of the LEARNER, D-LEARNER, and truncated SVD approaches in the context of the data application.

Specifically, we performed a 5-fold cross-validation analysis in a similar manner as described in Section 2.3.1. The training and test sets were obtained by randomly partitioning the entries of Y_0 . We applied LEARNER to the training data as described in Section 2.3. We also applied a missing value SVD approach – also referred to as hard thresholding [5] – to the (target population) training data. This approach numerically solves the following optimization problem

$$W_{0,r} := \arg \min_{W: \text{rank}(W)=r} \sum_{(i,j) \in \Omega_k} (W_{ij} - Y_{0,ij})^2 \tag{7}$$

where Ω_k denotes the set of the indices corresponding to the k th training data set. Numerical approaches to solve (7) are described in Mazumder et al. [5]. We used the `softImpute` R package [38] to apply this approach. We applied the D-LEARNER approach as described in Section 2.4, using $W_{0,r}$ in place of Y_0 . Last, we applied the truncated SVD to the source population data (Y_1) to estimate Θ_0 . We used a rank of 8 for all approaches.

For each approach, we computed the MSE in the corresponding validation data, i.e.

$$\text{MSE}(\hat{\Theta}_0, k) = \frac{1}{|\Omega_k^\perp|} \sum_{(i,j) \in \Omega_k^\perp} (\hat{\Theta}_{0,ij} - Y_{0,ij})^2 \tag{8}$$

where $\hat{\Theta}_0$ denotes the estimator of Θ_0 and Ω_k^\perp denotes the set of the indices corresponding to the k th test data set.

The MSE results are given in Table 3. LEARNER had the smallest MSE in each of the test sets. D-LEARNER and the target population truncated SVD approaches performed similar to each other, and the source population truncated SVD approach performed worst. The relatively small differences in MSE between all the approaches may be attributed to using noisy “true” values when computing the MSE (i.e., using $Y_{0,ij}$ rather than $\Theta_{0,ij}$ in (8)).

Table 3: Results of the cross-validation analyses comparing LEARNER, D-LEARNER, and the truncated SVD approaches. The smallest MSE for each test set is in bold text.

Test Set	Mean Squared Error			
	LEARNER	D-LEARNER	SVD (Target)	SVD (Source)
1	1.11	1.15	1.15	1.40
2	1.11	1.15	1.14	1.40
3	1.11	1.16	1.15	1.40
4	1.11	1.15	1.15	1.39
5	1.11	1.16	1.15	1.41

Although LEARNER demonstrates empirical superiority over D-LEARNER in the holdout dataset, further external validation would be valuable, such as a larger meta-analysis of these genetic associations in an East Asian population or an evaluation from a disease risk prediction perspective using an external dataset from the same population.

5 Discussion

We proposed an approach that leverages data from a source population to improve estimation of a low-rank matrix in an underrepresented target population. This approach penalizes differences between the latent row and column spaces between the source and target populations. Further, we presented a cross-validation approach for selecting the degree of transfer learning between the populations. We also presented a corresponding tuning parameter free approach under the assumption of shared latent row and column spaces between the target and source populations. Our simulation and empirical evaluations illustrated that these approaches can effectively improve inference in the target population under various settings. These approaches are implemented in the R package `learner`, available on GitHub at <https://github.com/stmcg/learner>.

Our data application focused on the problem of estimating genetic associations across different phenotypes, which can ultimately be used in disease risk prediction as well as in clustering diseases and genetic variants [12, 11]. Although underrepresentation of target populations and heterogeneity across populations are well-known problems in this literature [19, 18], statistical methods adopting a transfer learning approach have not been applied in this context to the best of our knowledge.

Several modifications to the proposed methodology could enhance the flexibility or performance of LEARNER’s application. First, as we discussed in Section 2, column- and row-space specific penalties can be added when the degrees of similarity in the latent row and column spaces between the source and target populations are believed to be highly different. Second, selection of the rank in each population can be done separately when needed. Additionally, one may consider extensions for the setting with multiple different source populations. For example, under the assumption that the source populations have the same latent spaces, one could pool information across the sources to better estimate the projection matrices onto the latent factors. Indeed, Shi and Al Kontar [28] and Li et al. [29] adopted similar ideas in multi-source PCA contexts. Fourth, adaptations to account for heteroskedastic noise may be considered when estimating latent subspaces or determining rank. Previous research indicates that heteroskedastic noise can substantially affect the accuracy of conventional spectral decomposition methods [39]. Incorporating techniques that address heteroskedasticity into the LEARNER algorithm could improve its performance [39, 40].

Acknowledgements

Sean McGrath was supported by the National Science Foundation Graduate Research Fellowship Program under Grant No. DGE2140743. Rui Duan was supported by National Institutes of Health (R01 GM148494).

References

- [1] Laurens Van Der Maaten, Eric O Postma, H Jaap Van Den Herik, et al. Dimensionality reduction: A comparative review. *Journal of machine learning research*, 10(66-71):13, 2009.
- [2] Laura Lazzeroni and Art Owen. Plaid models for gene expression data. *Statistica sinica*, pages 61–86, 2002.
- [3] Emmanuel Candes and Benjamin Recht. Exact matrix completion via convex optimization. *Communications of the ACM*, 55(6):111–119, 2012.
- [4] Emmanuel J Candès and Terence Tao. The power of convex relaxation: Near-optimal matrix completion. *IEEE transactions on information theory*, 56(5):2053–2080, 2010.
- [5] Rahul Mazumder, Trevor Hastie, and Robert Tibshirani. Spectral regularization algorithms for learning large incomplete matrices. *The Journal of Machine Learning Research*, 11:2287–2322, 2010.
- [6] Jian-Feng Cai, Emmanuel J Candès, and Zuowei Shen. A singular value thresholding algorithm for matrix completion. *SIAM Journal on optimization*, 20(4):1956–1982, 2010.
- [7] Tomas Mikolov. Efficient estimation of word representations in vector space. *arXiv preprint arXiv:1301.3781*, 3781, 2013.
- [8] Tomas Mikolov, Ilya Sutskever, Kai Chen, Greg S Corrado, and Jeff Dean. Distributed representations of words and phrases and their compositionality. *Advances in neural information processing systems*, 26, 2013.
- [9] Zheng Tracy Ke and Minzhe Wang. Using svd for topic modeling. *Journal of the American Statistical Association*, 119(545):434–449, 2024.
- [10] Edward J Hu, Yelong Shen, Phillip Wallis, Zeyuan Allen-Zhu, Yuanzhi Li, Shean Wang, Lu Wang, and Weizhu Chen. Lora: Low-rank adaptation of large language models. *arXiv preprint arXiv:2106.09685*, 2021.
- [11] Yosuke Tanigawa, Jiehan Li, Johanne M Justesen, Heiko Horn, Matthew Aguirre, Christopher De-Boever, Chris Chang, Balasubramanian Narasimhan, Kasper Lage, Trevor Hastie, et al. Components of genetic associations across 2,138 phenotypes in the uk biobank highlight adipocyte biology. *Nature communications*, 10(1):4064, 2019.
- [12] Saori Sakaue, Masahiro Kanai, Yosuke Tanigawa, Juha Karjalainen, Mitja Kurki, Seizo Koshiba, Akira Narita, Takahiro Konuma, Kenichi Yamamoto, Masato Akiyama, et al. A cross-population atlas of genetic associations for 220 human phenotypes. *Nature genetics*, 53(10):1415–1424, 2021.
- [13] Carl Eckart and Gale Young. The approximation of one matrix by another of lower rank. *Psychometrika*, 1(3):211–218, 1936.
- [14] Per Christian Hansen. The truncated svd as a method for regularization. *BIT Numerical Mathematics*, 27:534–553, 1987.
- [15] Ian T Jolliffe. *Principal component analysis for special types of data*. Springer, 2002.

- [16] Daniel D Lee and H Sebastian Seung. Learning the parts of objects by non-negative matrix factorization. *nature*, 401(6755):788–791, 1999.
- [17] Kathleen McGlone West, Erika Blacksher, and Wylie Burke. Genomics, health disparities, and missed opportunities for the nation’s research agenda. *Jama*, 317(18):1831–1832, 2017.
- [18] Alicia R Martin, Masahiro Kanai, Yoichiro Kamatani, Yukinori Okada, Benjamin M Neale, and Mark J Daly. Current clinical use of polygenic scores will risk exacerbating health disparities. *Nature genetics*, 51(4):584, 2019.
- [19] Segun Fatumo, Tinashe Chikowore, Ananyo Choudhury, Muhammad Ayub, Alicia R Martin, and Karoline Kuchenbaecker. A roadmap to increase diversity in genomic studies. *Nature medicine*, 28(2):243–250, 2022.
- [20] Karl Weiss, Taghi M Khoshgoftaar, and DingDing Wang. A survey of transfer learning. *Journal of Big data*, 3:1–40, 2016.
- [21] Yan Gao and Yan Cui. Deep transfer learning for reducing health care disparities arising from biomedical data inequality. *Nature communications*, 11(1):5131, 2020.
- [22] Tian Gu, Phil H Lee, and Rui Duan. Commute: communication-efficient transfer learning for multi-site risk prediction. *Journal of biomedical informatics*, 137:104243, 2023.
- [23] Sai Li, Tianxi Cai, and Rui Duan. Targeting underrepresented populations in precision medicine: A federated transfer learning approach. *The Annals of Applied Statistics*, 17(4):2970–2992, 2023.
- [24] Yuying Lu, Tian Gu, and Rui Duan. Enhancing genetic risk prediction through federated semi-supervised transfer learning with inaccurate electronic health record data. *Statistics in Biosciences*, pages 1–22, 2024.
- [25] Shigeyuki Oba, Motoaki Kawanabe, Klaus-Robert Müller, and Shin Ishii. Heterogeneous component analysis. *Advances in Neural Information Processing Systems*, 20, 2007.
- [26] Jianqing Fan, Dong Wang, Kaizheng Wang, and Ziwei Zhu. Distributed estimation of principal eigenspaces. *Annals of statistics*, 47(6):3009, 2019.
- [27] Junting Duan, Markus Pelger, and Ruoxuan Xiong. Target pca: Transfer learning large dimensional panel data. *Journal of Econometrics*, page 105521, 2023.
- [28] Naichen Shi and Raed Al Kontar. Personalized pca: Decoupling shared and unique features. *Journal of Machine Learning Research*, 25(41):1–82, 2024.
- [29] Zeyu Li, Kangxiang Qin, Yong He, Wang Zhou, and Xinsheng Zhang. Knowledge transfer across multiple principal component analysis studies. *arXiv preprint arXiv:2403.07431*, 2024.
- [30] Moritz Hardt. Understanding alternating minimization for matrix completion. In *2014 IEEE 55th Annual Symposium on Foundations of Computer Science*, pages 651–660. IEEE, 2014.
- [31] Wen Zhang, Xiang Yue, Weiran Lin, Wenjian Wu, Ruoqi Liu, Feng Huang, and Feng Liu. Predicting drug-disease associations by using similarity constrained matrix factorization. *BMC bioinformatics*, 19:1–12, 2018.
- [32] Lei Li, Zhen Gao, Yu-Tian Wang, Ming-Wen Zhang, Jian-Cheng Ni, Chun-Hou Zheng, and Yansen Su. Scmfmda: predicting microrna-disease associations based on similarity constrained matrix factorization. *PLoS computational biology*, 17(7):e1009165, 2021.
- [33] Raymond B Cattell. The scree test for the number of factors. *Multivariate behavioral research*, 1(2):245–276, 1966.

- [34] David Donoho, Matan Gavish, and Elad Romanov. Screenot: Exact mse-optimal singular value thresholding in correlated noise. *The Annals of Statistics*, 51(1):122–148, 2023.
- [35] Akiko Nagai, Makoto Hirata, Yoichiro Kamatani, Kaori Muto, Koichi Matsuda, Yutaka Kiyohara, Toshiharu Ninomiya, Akiko Tamakoshi, Zentaro Yamagata, Taisei Mushiroda, et al. Overview of the biobank japan project: Study design and profile. *Journal of epidemiology*, 27(Supplement.III):S2–S8, 2017.
- [36] Clare Bycroft, Colin Freeman, Desislava Petkova, Gavin Band, Lloyd T Elliott, Kevin Sharp, Allan Motyer, Damjan Vukcevic, Olivier Delaneau, Jared O’Connell, et al. The uk biobank resource with deep phenotyping and genomic data. *Nature*, 562(7726):203–209, 2018.
- [37] Mitja I Kurki, Juha Karjalainen, Priit Palta, Timo P Sipilä, Kati Kristiansson, Kati M Donner, Mary P Reeve, Hannele Laivuori, Mervi Aavikko, Mari A Kaunisto, et al. Finngen provides genetic insights from a well-phenotyped isolated population. *Nature*, 613(7944):508–518, 2023.
- [38] Trevor Hastie and Rahul Mazumder. *softImpute: Matrix Completion via Iterative Soft-Thresholded SVD*, 2021. R package version 1.4-1.
- [39] Anru R Zhang, T Tony Cai, and Yihong Wu. Heteroskedastic pca: Algorithm, optimality, and applications. *arXiv preprint arXiv:1810.08316*, 2018.
- [40] Boris Landa and Yuval Kluger. The dyson equalizer: Adaptive noise stabilization for low-rank signal detection and recovery. *arXiv preprint arXiv:2306.11263*, 2023.
- [41] Shaun Purcell, Benjamin Neale, Kathe Todd-Brown, Lori Thomas, Manuel AR Ferreira, David Bender, Julian Maller, Pamela Sklar, Paul IW De Bakker, Mark J Daly, et al. Plink: a tool set for whole-genome association and population-based linkage analyses. *The American journal of human genetics*, 81(3):559–575, 2007.
- [42] The 1000 Genomes Project Consortium. A global reference for human genetic variation. *Nature*, 526(7571):68–74, 2015.
- [43] Susan Fairley, Ernesto Lowy-Gallego, Emily Perry, and Paul Flicek. The International Genome Sample Resource (IGSR) collection of open human genomic variation resources. *Nucleic acids research*, 48(D1):D941–D947, 2020.

A Additional details on the simulation study

A.1 Hyperparameter settings

Recall that LEARNER involves specifying candidate λ_1, λ_2 values as well as several hyperparameters for the numerical optimization algorithm (i.e., initial values, step size, maximum number of iterations, tolerance for $|\epsilon_t - \epsilon_{t-1}|$). In this subsection, we describe the hyperparameter values used in the simulations.

In all simulation scenarios, we initialized U by $\hat{U}_1 \hat{\Lambda}_1^{1/2}$ and initialized V^\top by $\hat{\Lambda}_1^{1/2} \hat{V}_1^\top$. We set the tolerance for $|\epsilon_t - \epsilon_{t-1}|$ to be 0.001 and set the maximum number of iterations to 75. We considered 5 candidate λ_1 values in an equally spaced grid on the log scale (lower and upper bounds are described below). Similarly, we considered 5 candidate λ_2 values in an equally spaced grid on the log-scale, resulting in 25 candidate values for (λ_1, λ_2) .

The step size and grid of values for λ_1, λ_2 depended on the simulation scenarios. In general, we set the step size to a value where the optimization algorithm clearly converged in most iterations, and we set the upper and lower bounds for λ_1 and λ_2 to values so that the selected (λ_1, λ_2) fell well within the boundary of the grid in most iterations. Specifically, in the independent noise simulations, we set these parameters as follows:

- High similarity scenarios: We used a step size of $c = 0.0035$. The candidate λ_1 and λ_2 values ranged from 10^{-4} to 10^4 .
- Moderate similarity scenarios: We used a step size of $c = 0.035$. The candidate λ_1 values ranged from 10^0 to 10^4 , and the candidate λ_2 values ranged from 10^{-2} to 10^1 .
- Low similarity scenarios: We used a step size of $c = 0.07$. The candidate λ_1 values ranged from 10^0 to 10^4 , and the candidate λ_2 values ranged from 10^{-2} to 10^1 .

In the correlated noise simulations, we used a step size of $c = 0.035$. The candidate λ_1 and λ_2 values ranged from 10^{-4} to 10^4 .

Recall that LEARNER uses ScreenNOT for rank selection. ScreenNOT requires specifying one hyperparameter: a loose upper bound on the rank r . We set this value to $\lfloor \min\{p, q\}/3 \rfloor = 16$ in all simulation scenarios.

A.2 Selecting the degree of transfer learning based on an external data set

In this subsection, we consider a different approach for selecting the nuisance parameters (λ_1, λ_2) for LEARNER. This is motivated by the observation that the cross-validation approach described in the main text for selecting (λ_1, λ_2) can perform sub-optimally in the presence of correlated noise. The approach we consider here is based on using an external data rather than held out entries of Y_0 to estimate the MSE of LEARNER for each candidate (λ_1, λ_2) . We then apply this approach in the correlated noise simulation settings described in the main text.

A.2.1 Method

Suppose that we observe $Y_0^{\text{ext}} \in \mathbb{R}^{p \times q}$ in an external data set such that

$$Y_0^{\text{ext}} = \Theta_0 + Z_0^{\text{ext}} \quad (9)$$

where Z_0^{ext} follows the same distribution as Z_0 . The matrix Y_0^{ext} may have p' missing rows and q' missing columns due to inconsistencies between the measured variables in the data sources (e.g., the external source may not collect data on some of the phenotypes and genotypes that were included in Y_0 and Y_1). For each candidate (λ_1, λ_2) pair, we apply LEARNER (based on Y_0 and Y_1) and evaluate its MSE using the external data set, i.e.,

$$\text{MSE}(\lambda_1, \lambda_2) = \frac{1}{|\Omega_{Y_0^{\text{ext}}}|} \sum_{(i,j) \in \Omega_{Y_0^{\text{ext}}}} (\hat{\Theta}_{ij}^{\text{LEARNER}, \lambda_1, \lambda_2} - Y_{0,ij}^{\text{ext}})^2.$$

where $\hat{\Theta}^{\text{LEARNER}, \lambda_1, \lambda_2}$ denotes the LEARNER estimate with (λ_1, λ_2) and $\Omega_{Y_0^{\text{ext}}}$ denotes the set of non-missing entries in Y_0^{ext} . We select the value of (λ_1, λ_2) with the smallest MSE.

A.2.2 Simulation study

We apply this version of LEARNER in the simulation study described in Section 3.2 of the main text (i.e., with correlated noise). We generated Y_0^{ext} by equation (9).

The simulation results are summarized in Figure 8. LEARNER generally outperformed or performed comparable to the target-only SVD and D-LEARNER methods. As the degree of correlation increased, the discrepancy between the LEARNER and D-LEARNER methods generally decreased.

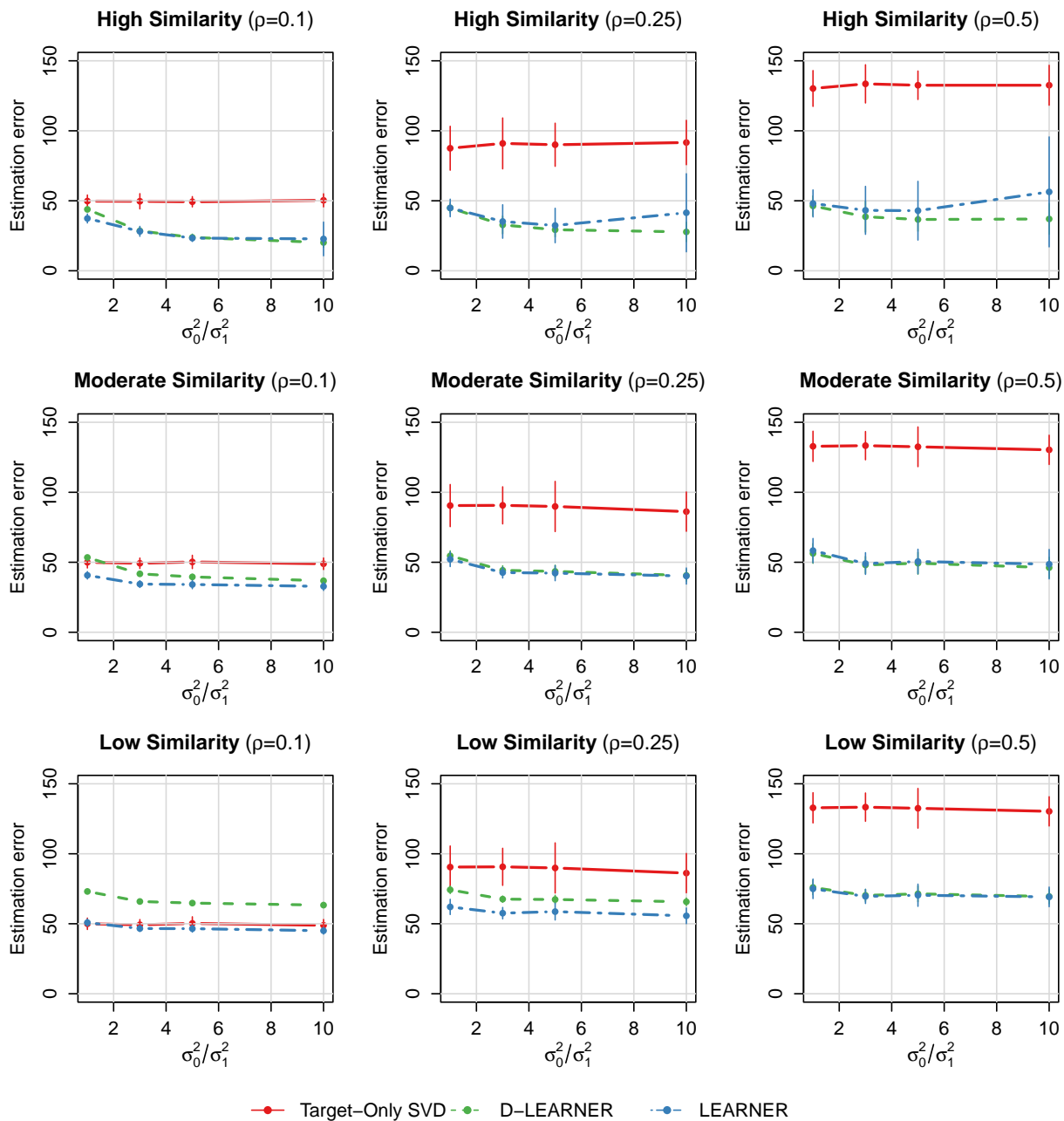


Figure 8: Simulation results under the correlated noise settings, where LEARNER used an external data set to select (λ_1, λ_2) . The error bars correspond to the standard deviation of the estimation error across the 50 repetitions.

B Additional details on the data application

B.1 Data processing

In this section, we describe the additional data processing steps that were performed after obtaining the GWAS summary statistics from Sakaue et al. [12]

We performed a variant screening procedure similar to that described by Sakaue et al.[12]. Specifically, we removed variants located in the major histocompatibility complex region (chromosome 6: 25–34 megabase). We considered estimates insignificant when either the p-value for a standard Wald test was greater than 0.001 or the standard error was greater than 0.2. We excluded variants that had all insignificant associations across the 145 phenotypes in either the BBJ or European populations. A total of 208,583 variants were left after this screening step. We then performed linkage disequilibrium (LD) pruning using PLINK[41] ('-indep-pairwise 50 5 0.1') with an LD reference from the 1000 Genomes Project phase 3 data[42, 43]. This resulted in 27,686 remaining genetic variants. We then removed 572 of these genetic variants because they had missing genetic association values across all of the 27 phenotypes that were only measured in the UKB data and not the FinnGen data. The final analytic data sets contained 27,124 genetic variants and 145 phenotypes, where there were 0.006% missing entries in Y_0 and 0.102% missing entries in Y_1 . These missing entries were set to 0 for all methods for consistency.

After performing the variant screening, we standardized the genetic associations. We used the 1000 Genomes Project phase 3 data as the Minor Allele Frequency (MAF) standardization reference. If the MAF of a variant in a given population is p , then the MAF standardization coefficient is $\sqrt{p(1-p)}$. Among the 2504 individuals in the 1000 Genomes Project phase 3 data, 504 are of eastern Asian ancestry and 503 are of European ancestry. We calculated the MAF values based on these individuals.

B.2 Exploratory Data Analyses

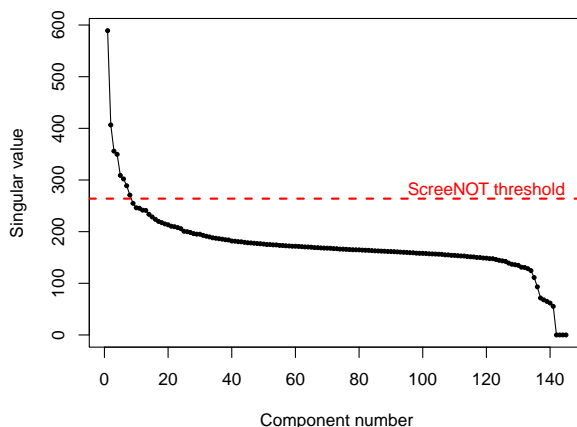


Figure 9: Scree plot based on the source population data.

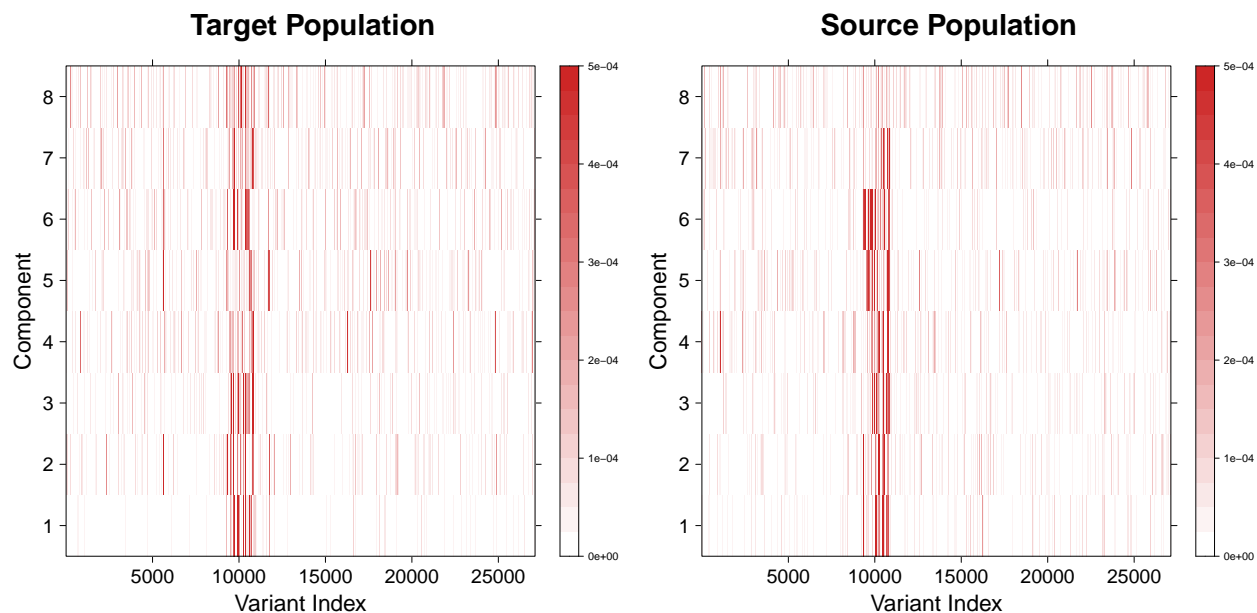


Figure 10: Heatmap of the matrix of variant contribution scores in the target population (left panel) and source population (right panel). The variants are ordered based on their chromosome and position number.

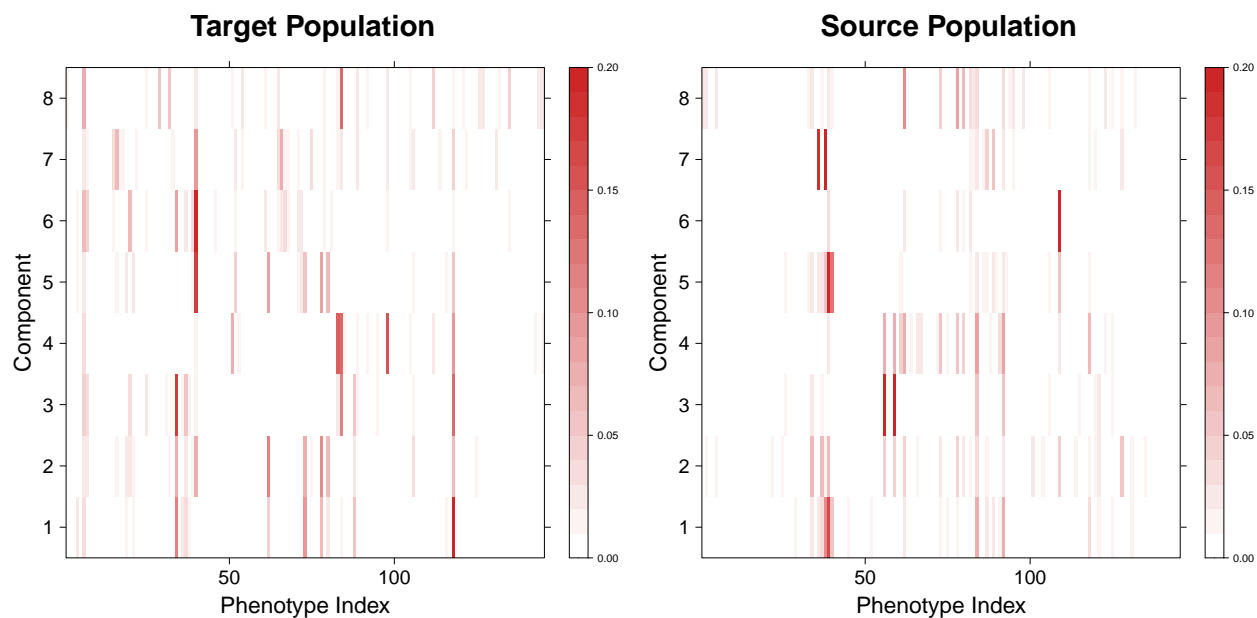


Figure 11: Heatmap of the matrix of phenotype contribution scores in the target population (left panel) and source population (right panel). The phenotypes are ordered based on their ICD-10 category.

Table 4: Top phenotypes in each latent factor in the source population. For each latent factor, we list the five phenotypes with the highest contribution scores. The phenotype contribution scores are in parentheses. The phenotypes related to the latent factor characterization are in bold text.

Factor	Characterization	Top phenotypes
1	Endocrine disorders	Type 1 diabetes (0.17) , hypothyroidism (0.11) , asthma (0.08), pediatric asthma (0.07), type 2 diabetes (0.05)
2	Autoimmune disorders	Type 1 diabetes (0.07) , Graves' disease (0.07) , hyperthyroidism (0.07) , IgA Nephritis (0.06) , angina pectoris (0.05)
3	Eye disorders	Uveitis (0.30) , iritis (0.30) , asthma (0.05), pediatric asthma (0.05), Graves' disease (0.02)
4	Asthma	Pediatric asthma (0.09) , asthma (0.08) , iritis (0.08), uveitis (0.08), angina pectoris (0.07)
5	Endocrine disorders	Type 1 diabetes (0.27) , type 2 diabetes (0.13) , psoriasis vulgaris (0.06), hypothyroidism (0.05) , asthma (0.03)
6	Psoriasis vulgaris	Psoriasis vulgaris (0.64) , type 1 diabetes (0.03), angina pectoris (0.03), varicose (0.02), stable angina pectoris (0.02)
7	Hypothyroidism	Hypothyroidism (0.35) , Hashimoto's disease (0.18) , chronic obstructive pulmonary disease (0.05), chronic bronchitis (0.05), IgA nephritis (0.02)
8	Angina pectoris	Angina pectoris (0.10) , stable angina pectoris (0.09) , unstable angina pectoris (0.06) , myocardial infarction (0.04), pediatric asthma (0.04)

Table 5: Top phenotypes in each latent factor in the target population. For each latent factor, we list the five phenotypes with the highest contribution scores. The phenotype contribution scores are in parentheses. The phenotypes related to the latent factor characterization are in bold text.

Factor	Characterization	Top phenotypes
1	Autoimmune disorders	Rheumatoid arthritis (0.23) , Graves' disease (0.11) , myocardial infarction (0.09), stable angina pectoris (0.07), chronic sinusitis (0.06)
2	Cardiovascular/metabolic disorders	Angina pectoris (0.11) , stable angina pectoris (0.11) , type 2 diabetes (0.08) , myocardial infarction (0.08) , Graves' disease (0.07)
3	Autoimmune disorders	Graves' disease (0.17) , rheumatoid arthritis (0.14) , asthma (0.12), chronic sinusitis (0.06), hyperthyroidism (0.05)
4	Respiratory/allergic disorders	Pollinosis (0.15) , allergic rhinitis (0.14) , asthma (0.13) , rheumatoid arthritis (0.10), allergic conjunctivitis (0.08)
5	Cardiovascular/metabolic disorders	Type 2 diabetes (0.18) , angina pectoris (0.09) , stable angina pectoris (0.08) , unstable angina pectoris (0.07) , myocardial infarction (0.06)
6	Type 2 diabetes	Type 2 diabetes (0.20) , Graves' disease (0.08), chronic hepatitis B (0.06), hepatic cancer (0.06), chronic hepatitis C (0.04)
7	Cardiovascular/metabolic disorders	Type 2 diabetes (0.09) , chronic heart failure (0.07) , cervical cancer (0.07), rheumatoid arthritis (0.04), cerebral aneurysm (0.04)
8	Unclear	Asthma (0.13), chronic hepatitis B (0.07), iron deficiency anemia (0.05), uterine fibroid (0.05), urticaria (0.05)

B.3 Hyperparameter settings for LEARNER

In this subsection, we describe the hyperparameters used for LEARNER in the data application.

We initialized U and V in the same manner as described in Appendix A. We also used the same tolerance for $|\epsilon_t - \epsilon_{t-1}|$. We considered 5 candidate values for λ_1 on an equally spaced grid on the log-scale, ranging from 10^0 to 10^4 . Similarly, we considered 5 candidate values for λ_2 on an equally spaced grid on the log-scale, ranging from $10^{-2.5}$ and $10^{2.5}$. We used a step size of 0.025 and a maximum number of iterations of 100. In the ScreeNOT approach for rank selection, we set the upper bound on the rank r to 35.

B.4 LEARNER Illustration

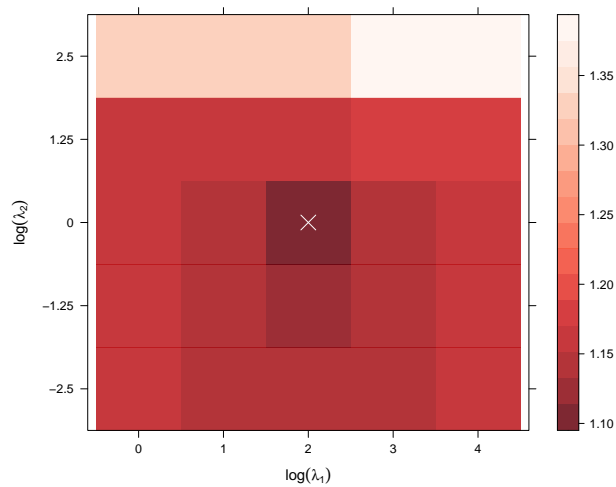


Figure 12: Heatmap of the held-out MSE for each candidate (λ_1, λ_2) . The white X mark indicates the candidate (λ_1, λ_2) with the smallest held-out MSE.

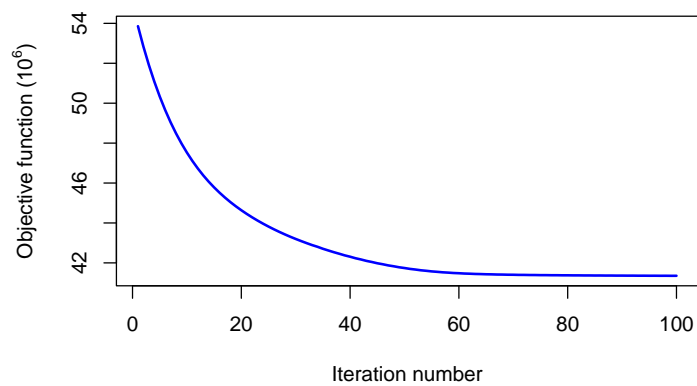


Figure 13: Convergence of the numerical optimization algorithm for solving equation (3).

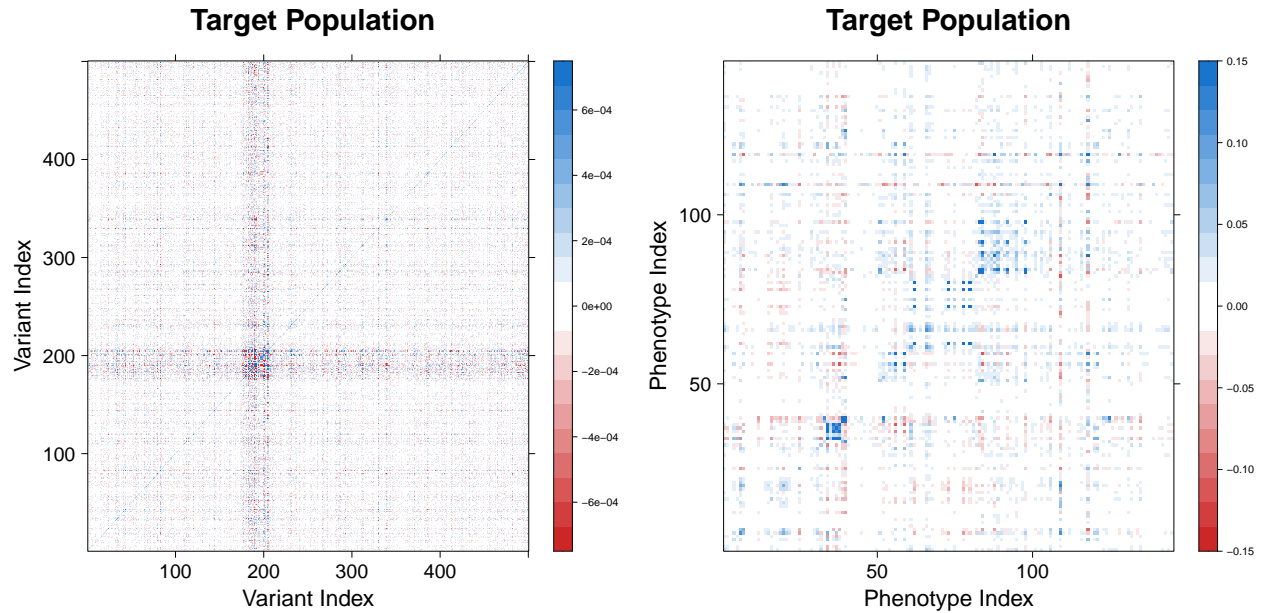


Figure 14: Heatmap of 500 randomly selected subset of rows and columns of $\mathcal{P}(\hat{V}_0^{\text{LEARNER}})$ (left panel) and $\mathcal{P}(\hat{U}_0^{\text{LEARNER}})$ (right panel). The phenotypes are ordered based on their ICD-10 category, and the 500 selected variants are ordered based on their chromosome and position number.

B.5 D-LEARNER Illustration

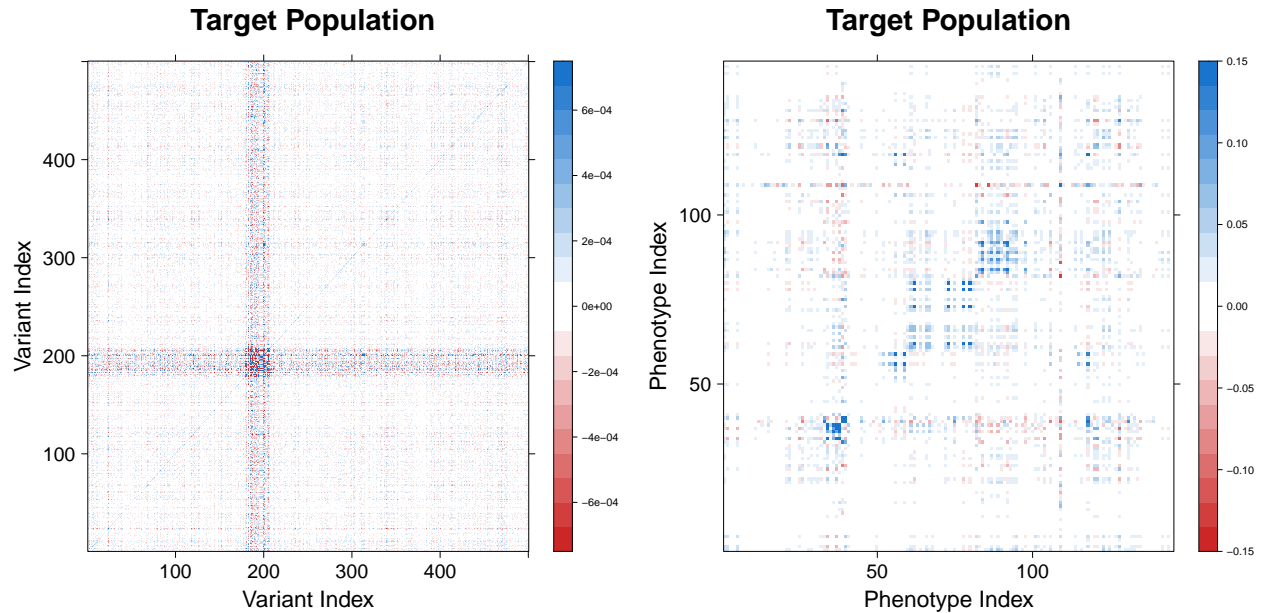


Figure 15: Heatmap of 500 randomly selected subset of rows and columns of $\mathcal{P}(\hat{V}_0^{\text{D-LEARNER}})$ (left panel) and $\mathcal{P}(\hat{U}_0^{\text{D-LEARNER}})$ (right panel). The phenotypes are ordered based on their ICD-10 category, and the 500 selected variants are ordered based on their chromosome and position number.